A FIELD STUDY OF EARTHQUAKE PREDICTION METHODS IN THE CENTRAL ALEUTIAN ISLANDS

(Part II)

C. Kisslinger, S. Billington, R. Bowman, S. Ihnen, G. Cruz
J. Pohlman, K. Sougstad and S. T. Morrissey

University of Colorado
CIRES
Boulder, Colorado 80302

USGS CONTRACT NO. 14-08-0001-19272
Supported by the EARTHQUAKE HAZARDS REDUCTION PROGRAM

OPEN-FILE NO. 81-937

U.S. Geological Survey
OPEN FILE REPORT

TABLE OF CONTENTS

TECHNICAL SUMMARY

Network Operation and Data Analysis.

The efforts made during 1979 and 1980 to harden the field installation against adverse weather in the Adak region are proving effective. A wind storm typical of those that had caused serious damage to the network in the past happened in December, 1980, with no effects noted. Two out of the 32 components monitored are out of service and will remain so until the stations can be reached by helicopter. The analogue magnetic tape recording system is working well.

Routine analysis of Adak network data was shifted to the use of digital data for all events since January 1, 1981. A number of problems have been made the full realization of this change difficult, but most of the routine work is being done from digital seismograms. Digitizing of the analogue tapes from the network is now routine on the PDP 11/34 and the tapes can be recycled to Adak in a timely way. The success of this approach depends critically on the reliability of the triggering algorithm which picks the events to be stored.

Program PING, developed at the University of Washington, has been modified to meet the needs of this project and is now used routinely for reading the seismograms. A useful change made was the addition of filtering to take out the severe wind noise which is often present in the data.

Investigations and Results.

Earthquake locations are complete for 1980 and a substantial part of the first few months of 1981. Monthly seismicity maps and graphs of cumulative numbers of earthquakes vs. time are routinely plotted as a means of displaying and monitoring space-time patterns of seismicity.

The cooperative study with the University of Texas, Galveston, based on simultaneous observations with their OBS and our island-based stations, is

nearly completed. The principal conclusions are:

1) Events located between a line about 100 km north of the trench axis and the volcanic islands are detected well by the island stations. Events southward from the trench axis are not recorded reliably by the island stations. These conclusions are based on a comparison of detections by the island and OBS stations.

2) Generally, the epicenters of events within the range of reliable detection by the island stations, calculated from island observations alone, are not far (about 3 km on average) from the locations based on the combined data set. However, the depths based on island data alone, especially for events deeper than 70 km, differ substantially from those based on the combined data set.

3) The flat-layer velocity model that has been used to locate Adak zone events seems to be satisfactory and no modifications have been required by the combined data.

The work still to be done is the completion of focal mechanism studies and cooperation with outside investigators using ray tracing techniques to test for mislocations and to explain the failure to detect on the islands the events seaward of the trench.

Computational procedures for calculating focal mechanisms from body-wave amplitude data are developed. These codes have been tested of several sets of real and synthetic data. Listings of the programs (Fortran for the Unix operating system on the PDP 11/70) are available on request.

Another case of re-orientation of the focal mechanism of small earthquakes before a larger one has been found. The earthquake, July 15, 1980, occurred very near to an event of February 22, 1976 that was throughly studied as part of this project. The earlier event not only showed a precursory change in focal mechanism orientation, but also was preceded by seismicity changes (3 1/2 months of quiescence followed by a burst of foreshocks). No patterns were seen

in the seismicity before the more recent earthquake. The focal mechanism change showed up primarily as a change in the ratio $(SV/P)_z$ at one station.

Reports.

Bowman, R., and C. Kisslinger (1981). Changes in focal mechanism of small earthquakes before an m_b 4.6 earthquake in the central Aleutian seismic zone (abstract), **Earthquake Notes, 52**, 69.

Chen, A. T., C. Frohlich, G. V. Latham, R. K. Cardwell, and S. Billington (1980). Is there seismic activity within the accretionary prism? (abstract), **EOS, 61**, 1044-1045.

Billington, S., E. R. Engdahl, and S. Price (1981). Changes in the seismicity and focal mechanism of small earthquakes prior to an M_S 6.7 earthquake in the central Aleutian island arc, in press, Ewing Series Vol. 4: **Earthquake Prediction.**

CHAPTER 1: NETWORK AND DIGITAL PROCESSING STATUS

Network Status.

The Adak seismic network is currently in good shape. Of the 32 components monitored (thirteen 2-component stations and one 6-component station), AD3 Z and AD6 H are not operational and cannot be repaired until the next time the field sites can be reached. In addition, in mid-April 1981 the observatory discriminator for AK5 Z failed. This unit is currently being repaired and is expected to be back in place within a month.

The good status of the network is especially noteworthy in light of a severe wind storm in the first week of December 1980. This was the first severe wind storm locally since the one of October 1977 which put half of the Adak network out of operation. During the summer of 1979, to make all of the stations more wind-resistant, the antennas were re-installed and the battery housings replaced at all sites. During the summer of 1980, a 30 ft. tower was erected on an exposed part of Adak Island to hold receiver antennas. Apparently none of the new installations were damaged in the December winds.

Recently a study was undertaken to determine the current status of station polarities for the Adak network. Seismograms of over 100 deep Tonga-Fiji earthquakes which occurred from August 1974 through January 1981 were examined. About one-third of them were useful for comparison of P-waveforms across the Adak network. The study showed that the polarity of the vertical component is currently reversed for two stations (AK1 and AK3). This polarity reversal was inadvertantly initiated during the 1979 summer field trip.

The 1980-1981 winter field trip took place in January 1981. A complete description of this field trip is being prepared as a special technical report by S. Morrissey.

Digital Data Analysis.

As of January 1, 1981, the data base form for the Adak project consists of analogue magnetic tapes instead of analogue (Develocorder) film records. Develocorder records are still being acquired concurrently with the magnetic tapes to provide back-up, and the Develocorders on Adak will eventually be run at either half-speed or for only half of the stations of the network.

The final hurdle in the conversion to the use of magnetic tape as the data base form was overcome when a satisfactory trigger algorithm was established for event detection. The trigger algorithm we use was developed by S. Malone and his colleagues at the University of Washington from an algorithm written by C. Johnson at Cal Tech. This algorithm had to be refined for use with the Adak stations. Parameters in the trigger algorithm were adjusted to yield the best sensitivity to seismic events without oversensitivity to background or electrical noise. The network was divided into six subnets each of approximately ten horizontal and vertical station components. Three subnets are composed of station components from the western, central, and eastern portions of the network, respectively, and the remaining three subnets contain a selection of station components which span the network and were chosen on the basis of their consistently superior level of detection. For an event to trigger the algorithm, a minimum of three members of any one subnet has to register a sudden increase in signal amplitude. Aside from the selection of the components for the subnets, there are several other adjustable parameters in the trigger algorithm. These were experimentally adjusted to obtain a satisfactory level of event detection. For example, the length of record for each trigger was halved to avoid missing earthquakes which follow a triggered event by two or three minutes.

In a survey of a five-day sample time period in February, 1981, a total of 32 local events, 27 regional events, and 3 teleseisms were found by the visual scan-

ning of Develocorder films by an experienced scanner. Of these, the trigger algorithm detected 19 local events, 12 regional events, one teleseism, and found two additional local events. Examination on the Develocorder films of the local events missed by the algorithm found them to be very small (magnitude too small to be determined by duration), and only two were conceivably locatable (with just four stations recording each).

PING is another of the programs originally developed at the University of Washington and substantially modified at CIRES for use with the Adak data. This program allows an observer to manipulate and read data from digital seimogram traces portrayed on an interactive graphics terminal. In its current implementation, PING allows the observer to: (1) pick P-wave arrival times; (2) indicate the first motions and whether the arrivals are emergent or impulsive; (3) indicate the quality of the picks by number (optional); (4) display vertical bars indicating the previous pick times over the trace; (5) do all of the above for the S-wave arrivals; (6) redisplay any portion of a trace with any combination of vertical or horizontal magnification; (7) hi-pass, lo-pass, or band-pass filter the seismograms; (8) do special cascaded hi-pass filtering to eliminate wind noise; (9) pick duration of codas for duration magnitude determination; (10) pick the amplitudes of P- and S-wave arrivals for $(SV/P)_z$ amplitude studies; (11) input comments on a line-by-line basis; and (12) determine the time corresponding to any point on a trace for special studies.

The cascaded filtering is one of the refinements of PING generated at CIRES. In the example of its use shown in Figure 1-1, wind noise recorded on the vertical component at station AD1 is filtered out so that the arrival time of the P-wave can be read. First motions are not read from digitally filtered data.

More types of data are now being routinely recorded for each earthquake than were when Develocorder films provided the data base form for the project.

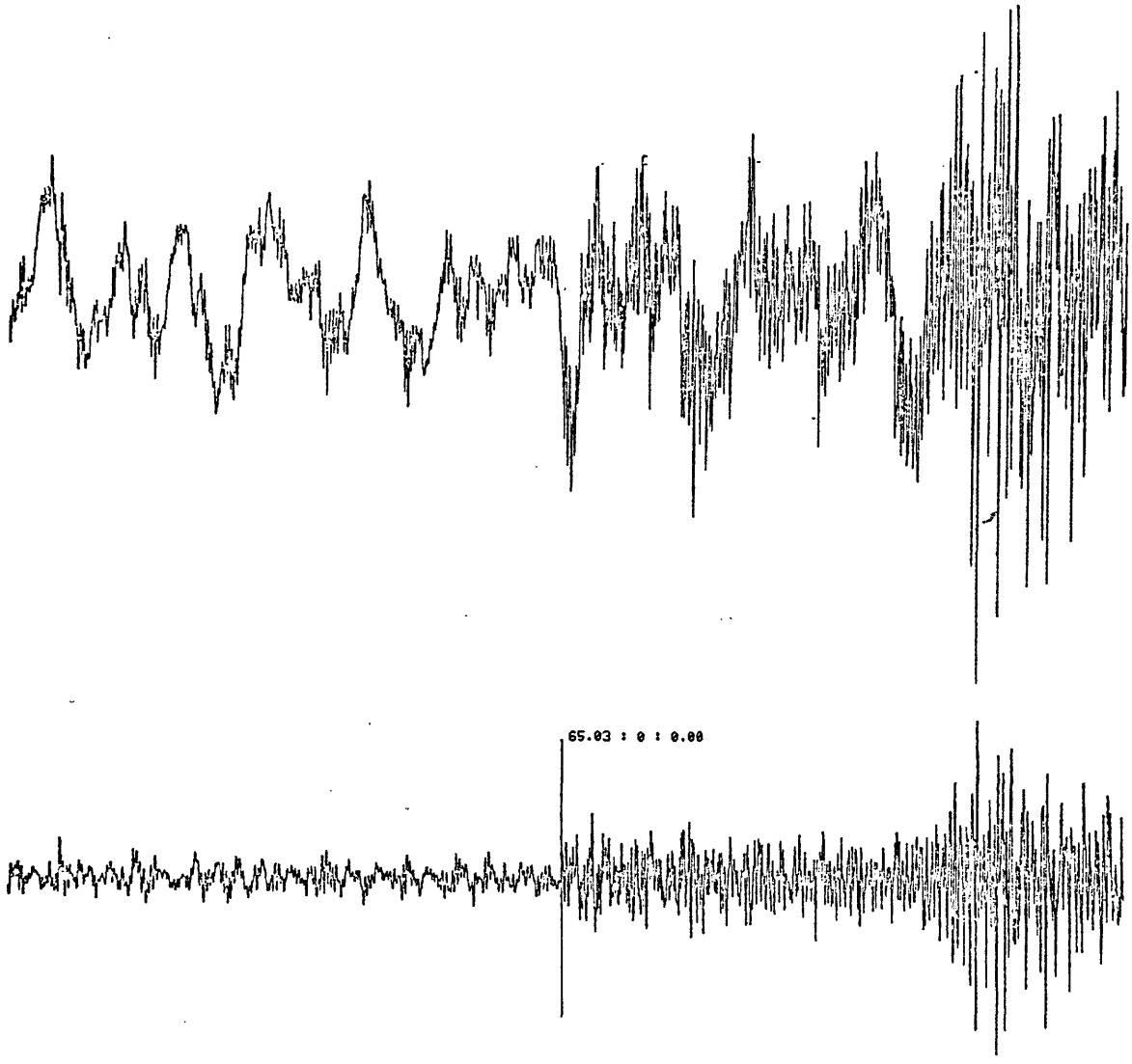

Figure 1-1: Illustration of digital filtering to improve signal characteristics on windy days. Both seismograms are for the same time period (about 25 seconds are shown) at station AD1Z. The top trace is the normal unfiltered seismogram; the bottom trace has been filtered. The verical line at the middle of the bottom trace was superimposed when the P-wave arrival time was picked.

Because of this, and because of the novelty of digital processing, hypocenter determinations now take longer than they did. As project personnel acquire experience with the digital system, we expect more efficiency in hypocenter determinations, but the need has developed for a full-time data manager to cope with the rest of the data manipulation.

CHAPTER 2: RECENT SEISMICITY

1169 earthquakes were located by the Adak local seismographic network in 1980 (Figure 2-1). The epicenters of all of these earthquakes are seen in Figure 2-2, and the seismic activity by month is seen for April through December in Figure 2-3. The largest earthquakes located by the Adak network during the year occurred on January 16 (m_b 5.8), February 6 (m_b 5.1), April 15 (m_b 5.0), July 5 (m_b 5.2), and November 21 (m_b 5.7). Of particular interest is an earthquake which occurred on July 15 (m_b 4.6) in very nearly the same location as the 1976 earthquake studied for precursors by Engdahl and Kisslinger (1977). A comparable study of the July 1980 earthquake is described later in this report. Another interesting feature in the seismicity near Adak this year is a burst of activity in August (Figure 2-3e) near 51.45° N and 176.30° W (in the source region we call "S1").

We also observe in 1980 a dramatic increase in the number of shallow back-arc earthquakes, starting in the spring of 1980. These occur most often between the historically active volcanoes monitored by the Adak seismic network: Great Sitkin, Kanaga, and Tanaga. No unusual volcanic activity has been observed on these islands during this time period, but Gareloi erupted in August 1980 (**EOS, 61**, p. 660, 1980, and **62**, p. 14, 1981). Gareloi is the next volcano to the west, located about 80 km from the westernmost Adak network station (on Tanaga). We have started a study of the spatial and temporal distribution of the shallow back-arc earthquakes, their focal mechanisms, and their possible interpretation in terms of volcanic activity.

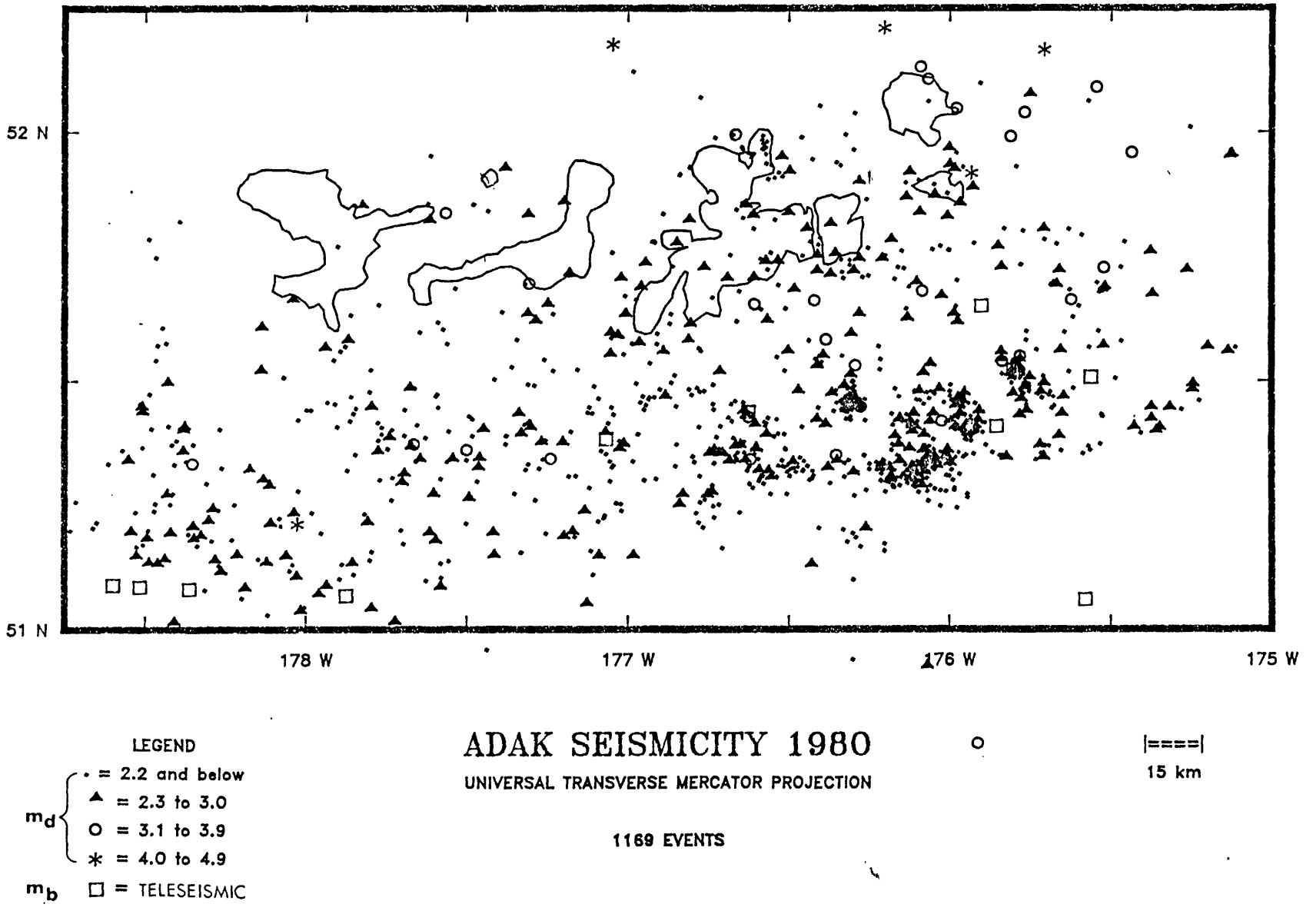

Figure 2-2: Map of seismicity near Adak which occurred during 1980. All epicenters were determined by the Adak network. Events marked with squares are those for which a teleseismic body-wave magnitude has been determined by the USGS; all other events are shown with symbols which indicate the duration magnitude determined by the Adak network. The islands mapped (from Tanaga on the west to Great Sitkin on the east) indicate the geographic extent of the Adak seismic network.

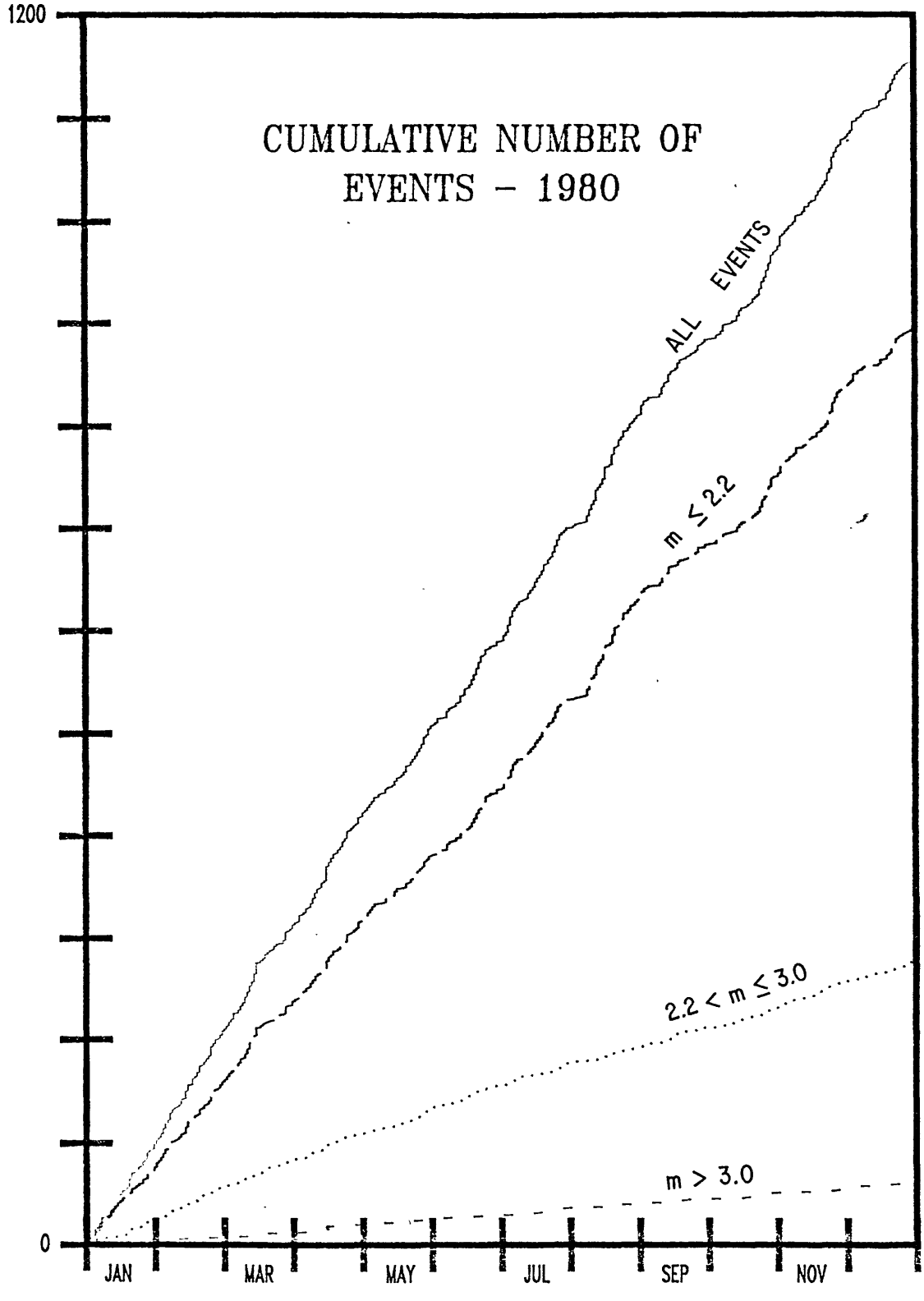

Figure 2-1: Plot of cumulative number of earthquakes as a function of time for 1980, broken down by arbitrary duration magnitude bands. Each unit on the vertical axis is 100 events.

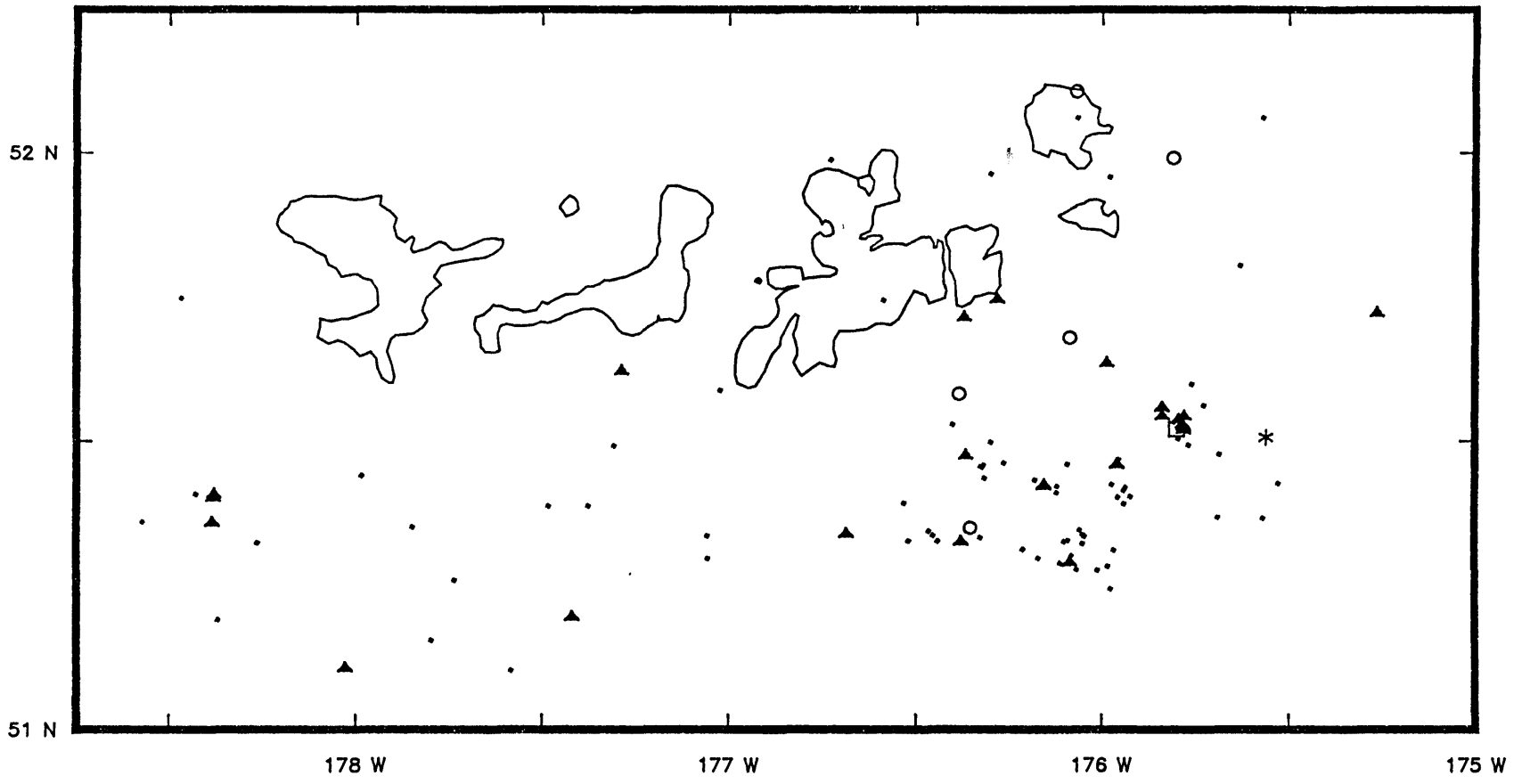

Figure 2-3a: Seismicity map for April 1980. Epicenters determined by the Adak network. The islands and epicenter symbols are as in Figure 2-2.

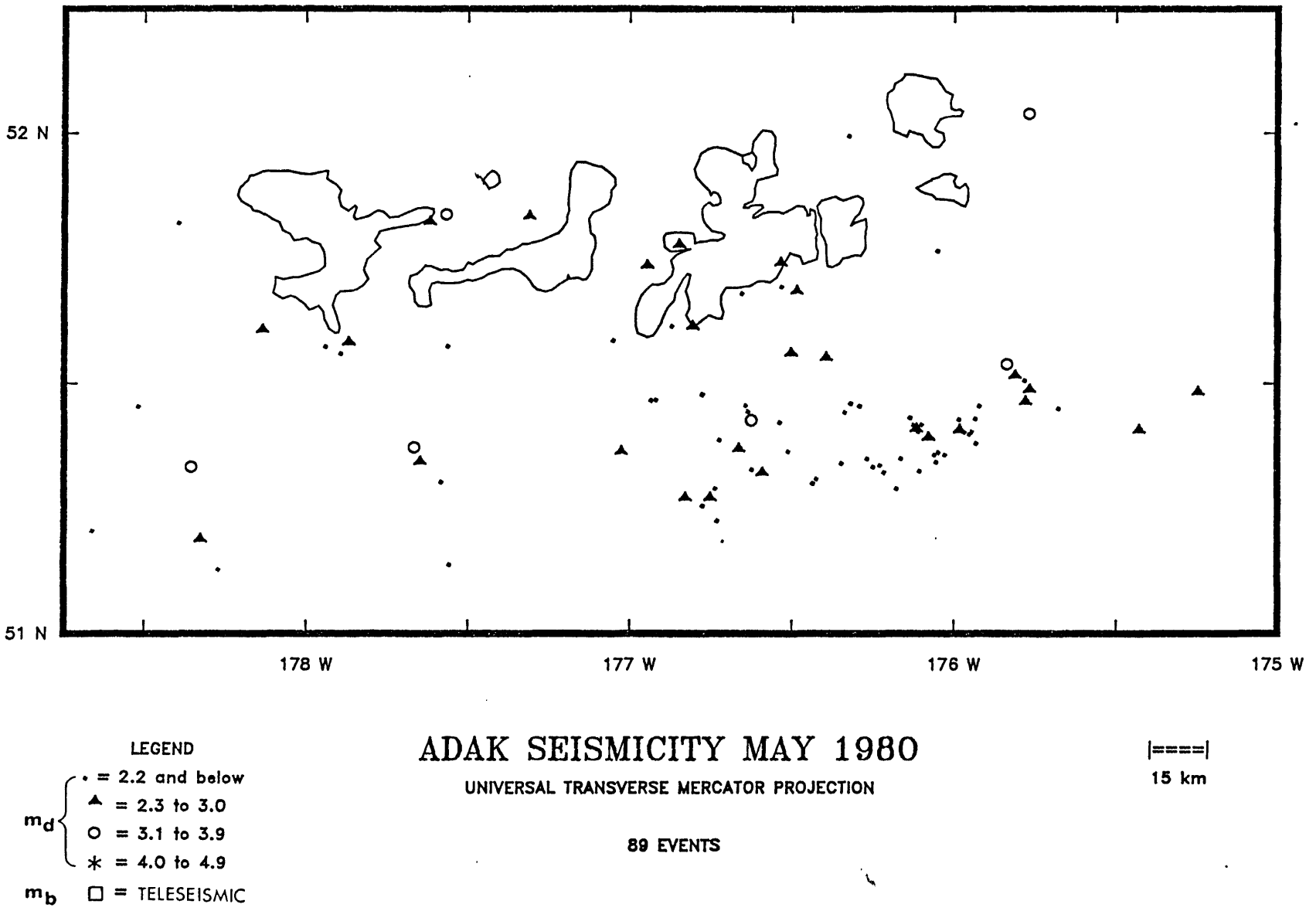

Figure 2-3b: Seismicity map for May 1980. Epicenters determined by the Adak network. The islands and epicenter symbols are as in Figure 2-2.

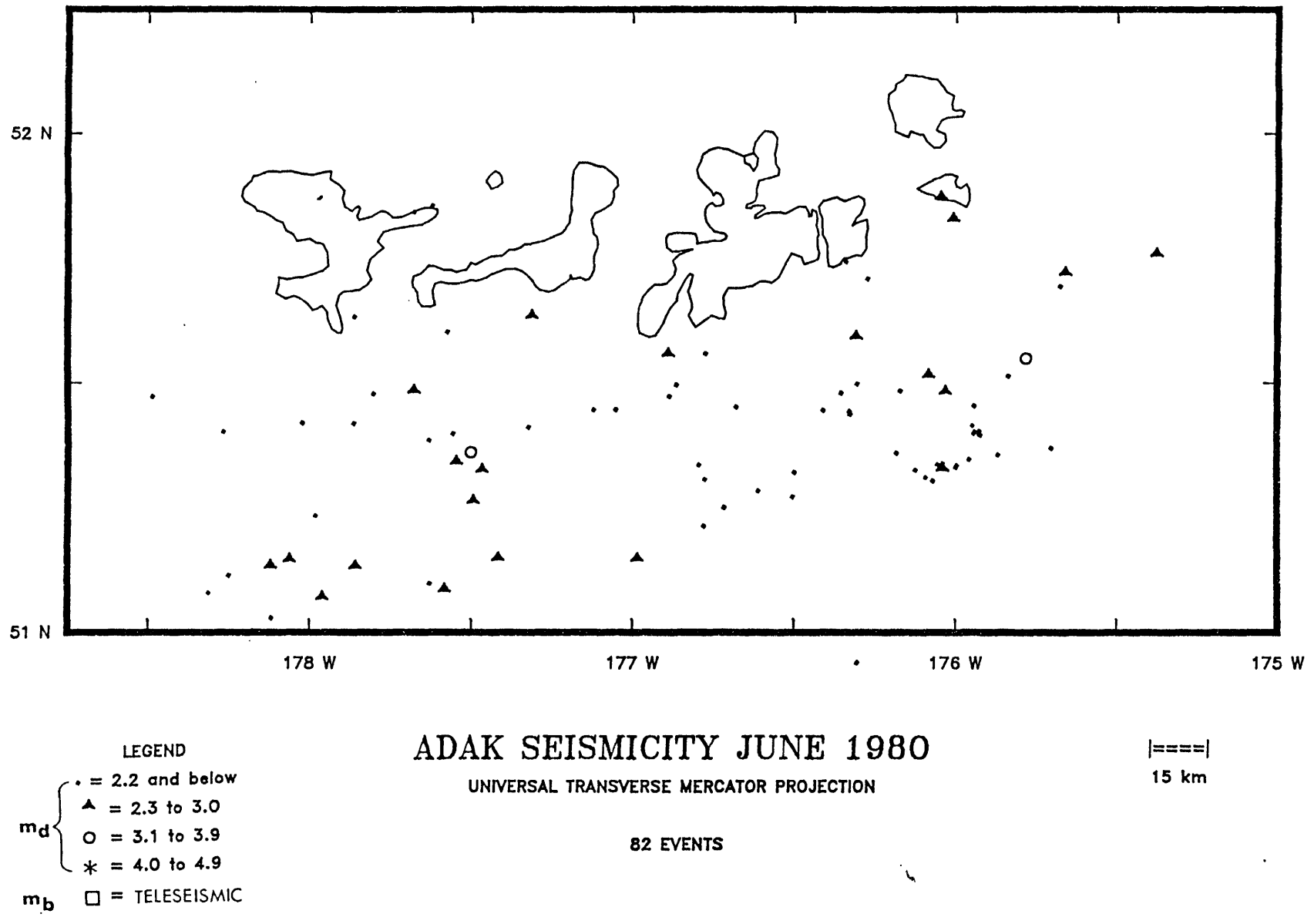

Figure 2-3c: Seismicity map for June 1980. Epicenters determined by the Adak network. The islands and epicenter symbols are as in Figure 2-2.

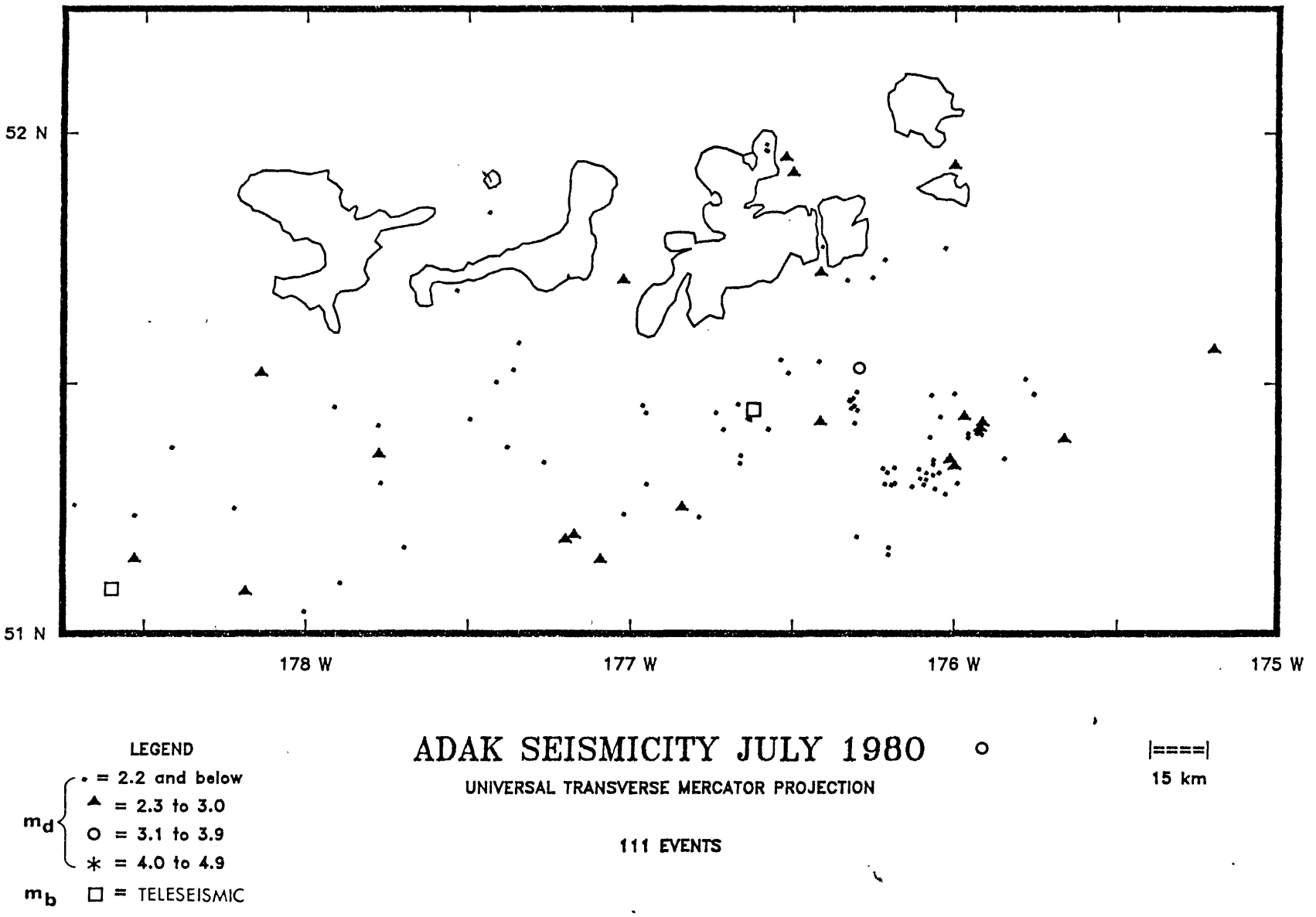

Figure 2-3d: Seismicity map for July 1980. Epicenters determined by the Adak network. The islands and epicenter symbols are as in Figure 2-2.

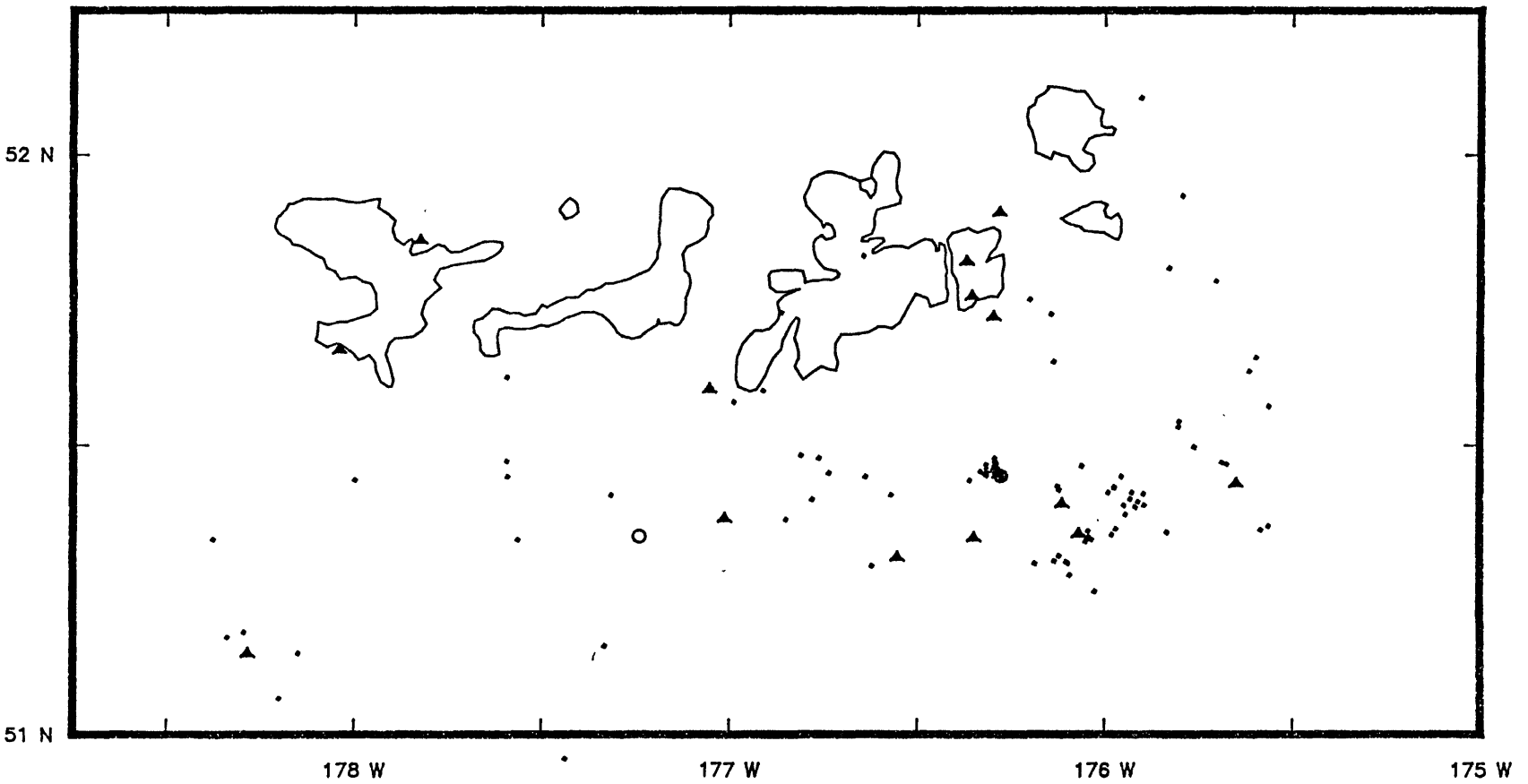

Figure 2-3e: Seismicity map for August 1980. Epicenters determined by the Adak network. Twenty-five events are located near 51.45°N and 176.30°W, 11 of which occurred on a single day. The islands and epicenter symbols are as in Figure 2-2.

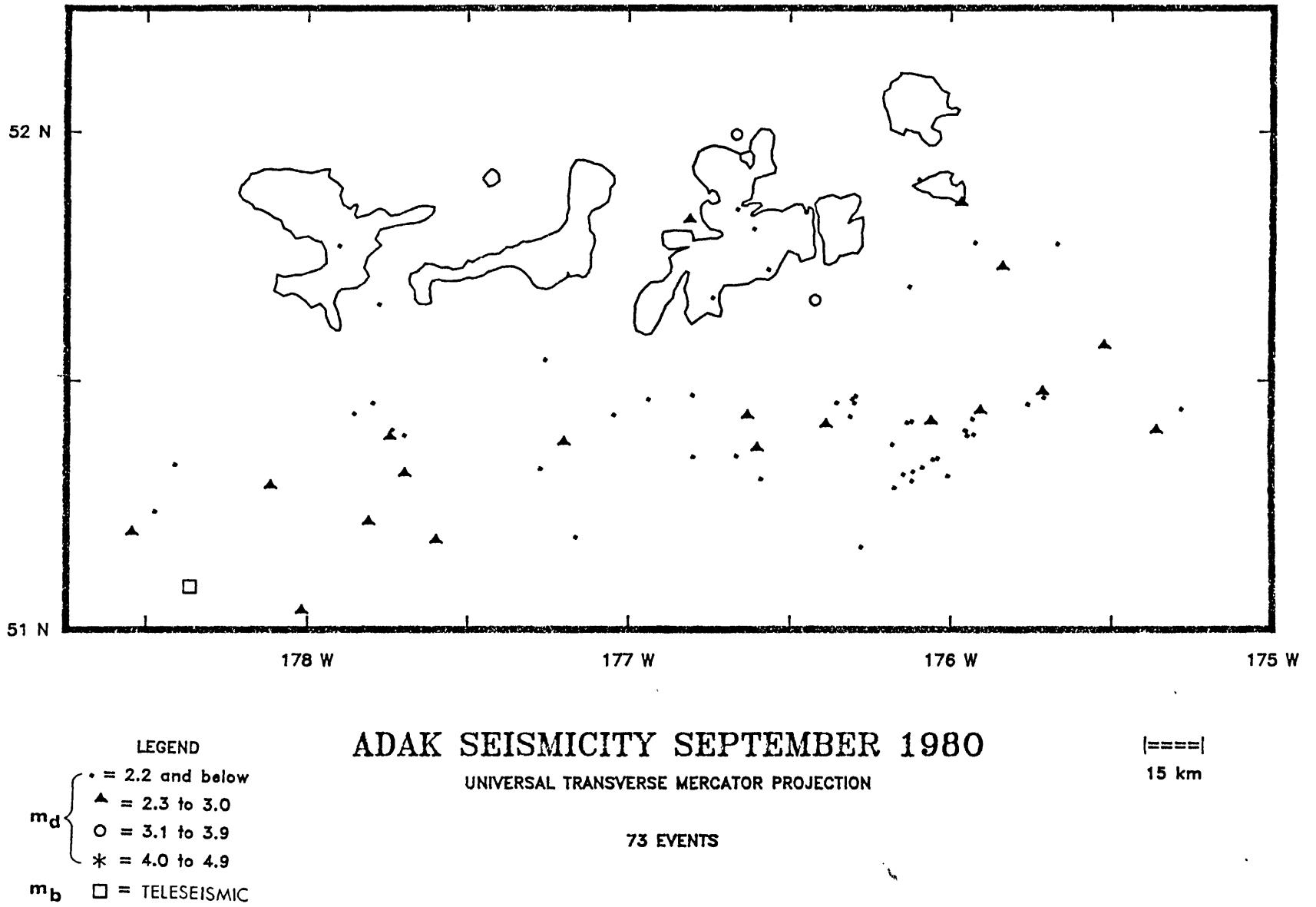

Figure 2-3f: Seismicity map for September 1980. Epicenters determined by the Adak network. The islands and epicenter symbols are as in Figure 2-2.

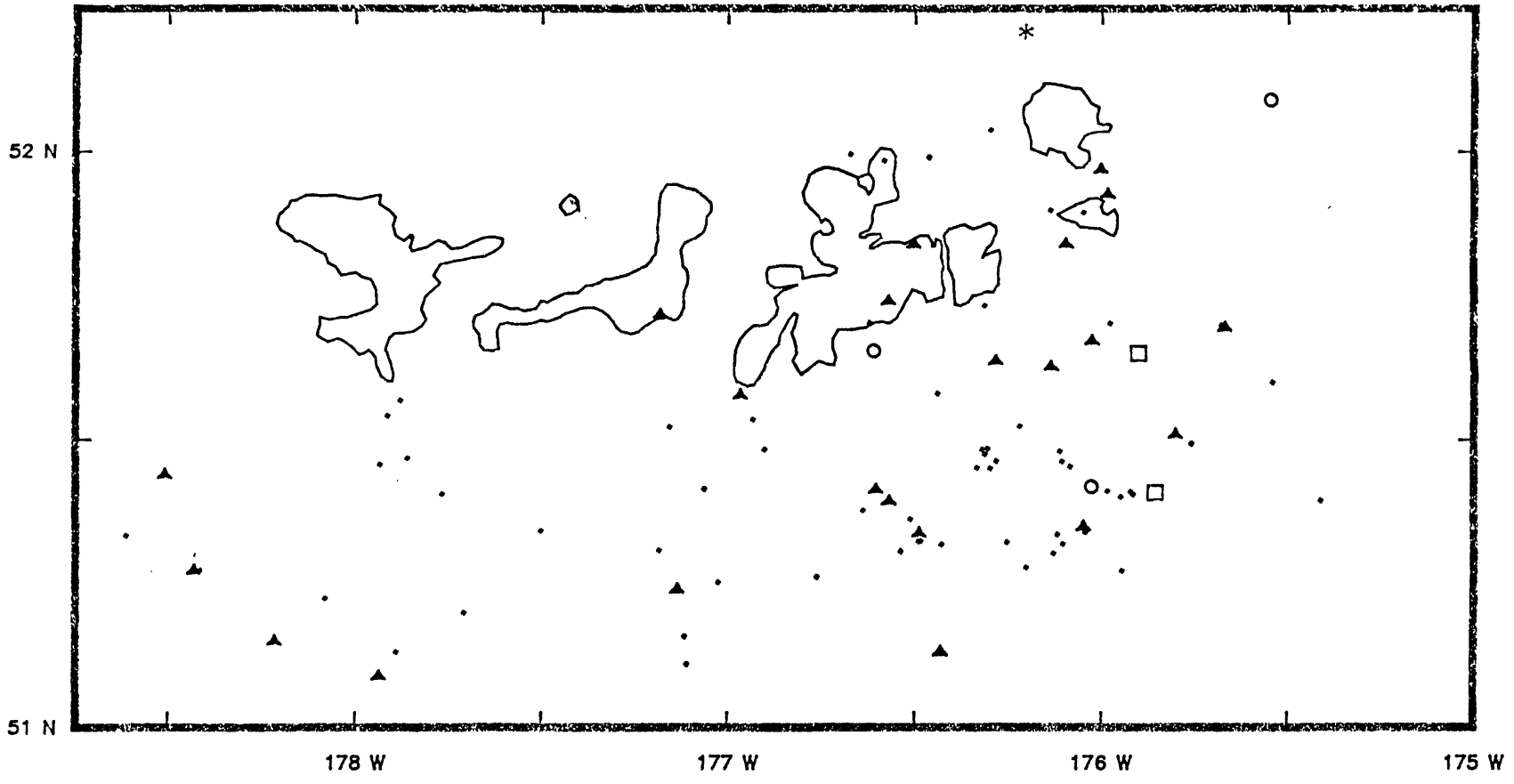

Figure 2-3g: Seismicity map for October 1980. Epicenters determined by the Adak network. The islands and epicenter symbols are as in Figure 2-2.

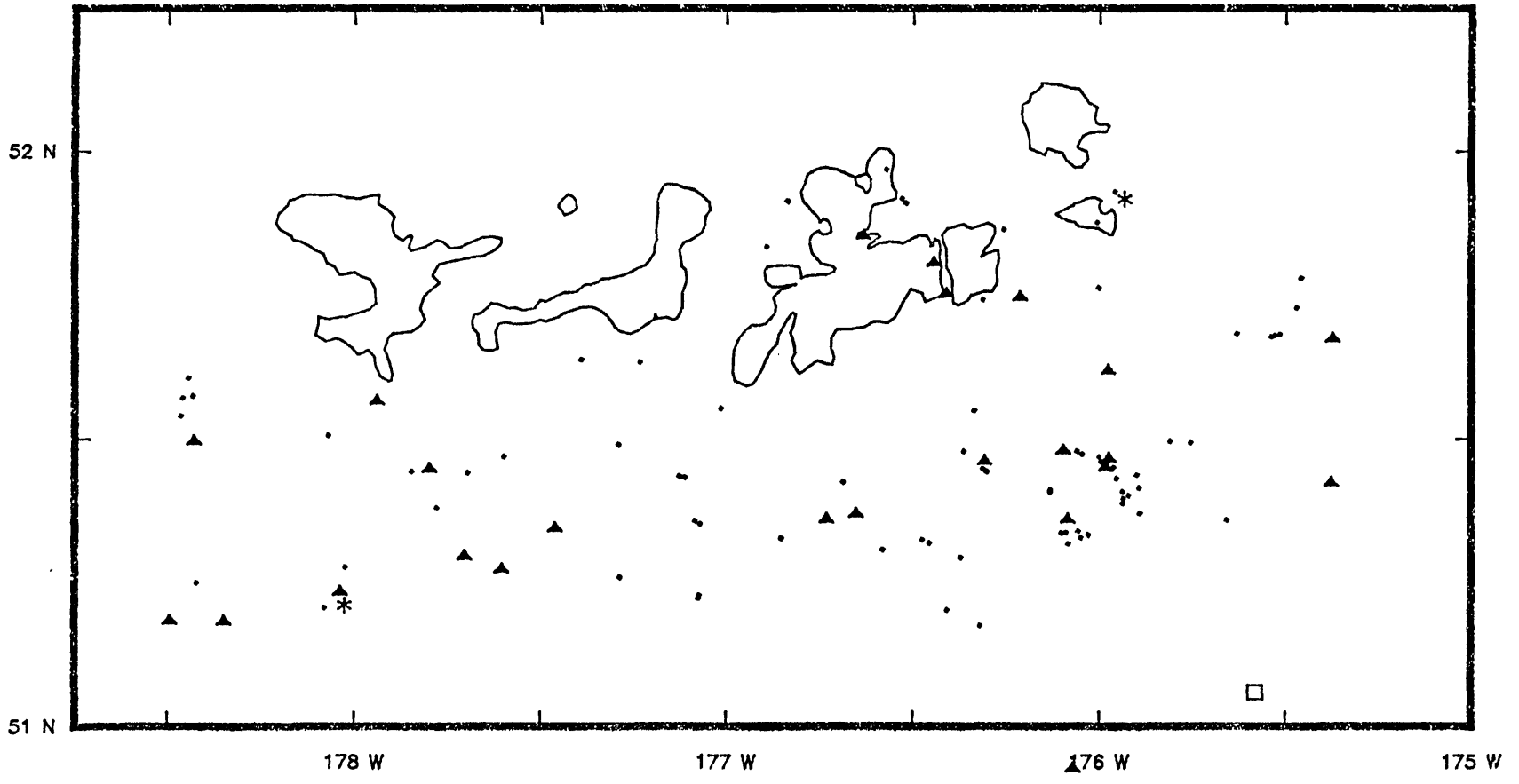

Figure 2-3h: Seismicity map for November 1980. Epicenters determined by the Adak network. The islands and epicenter symbols are as in Figure 2-2.

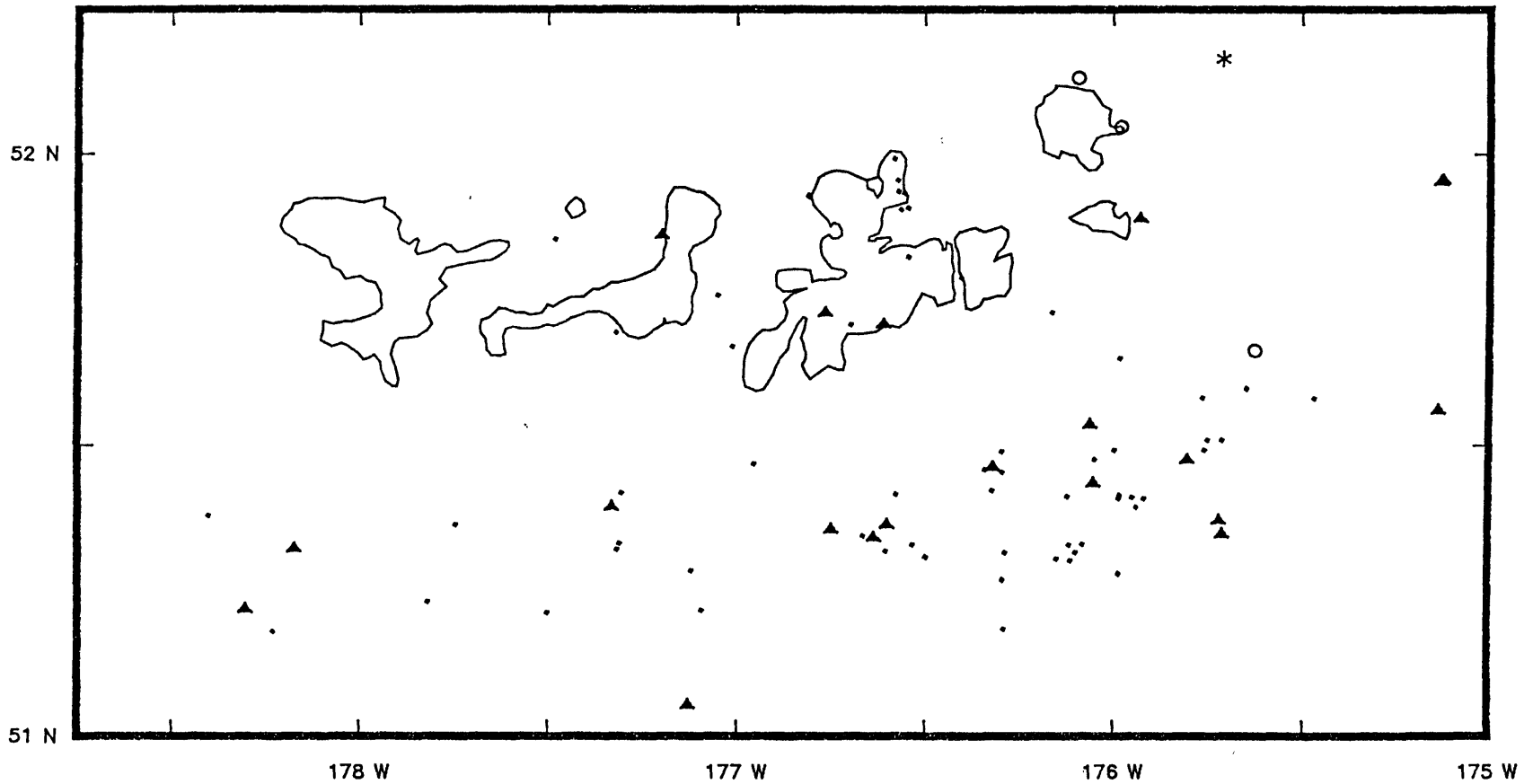

Figure 2-3i: Seismicity map for December 1980. Epicenters determined by the Adak network. The islands and epicenter symbols are as in Figure 2-2.

CHAPTER 3: DETECTION AND LOCATION OF EARTHQUAKES NEAR ADAK USING LAND AND OCEAN BOTTOM SEISMOGRAPH STATIONS

by Selena Billington

As part of a cooperative study with the Adak project, the Marine Science Institute of the University of Texas deployed ocean bottom seismograph (OBS) stations south of Adak for about a month during each of the summers of 1978 and 1979. The 1979 placement of the OBSs was seaward of the trench (Figure 3-1) and few events were recorded in common between the Adak land network and the OBS network (Frohlich et al., 1980). The joint study of the 1978 data is nearing completion; a paper describing both studies is expected to be ready for submission for publication in July.

Eight OBSs were successfully deployed and recovered in 1978 and nine in 1979 (Figure 3-1). During the times of both deployments, only seven Adak land stations were operating (Figure 3-1); the others were down due to a severe wind storm during the winter of 1977-1978. Despite this misfortune, the joint study has successfully answered the following important questions: (1) How good is the detection capability of the Adak land network for earthquakes under the Aleutian terrace or near the trench?; (2) how do the locations of earthquakes determined by the land network alone compare with those determined using stations located directly over the seismicity?; and (3) is there a substantially better flat-layer velocity model that should be used in routine locations of events by the Adak land stations? In addition, we are currently investigating the focal mechanisms of the (generally small) earthquakes in the study region in the light of the additional coverage of the focal sphere provided by the OBS stations.

Detection capability of the Adak land net. Results from both OBS deployments show that shallow earthquakes occur in two distinct groups. One group lies between the trench axis and a line about 60 km seaward of the axis (Frohlich et al., 1980). These events are generally not recorded by land and OBS stations

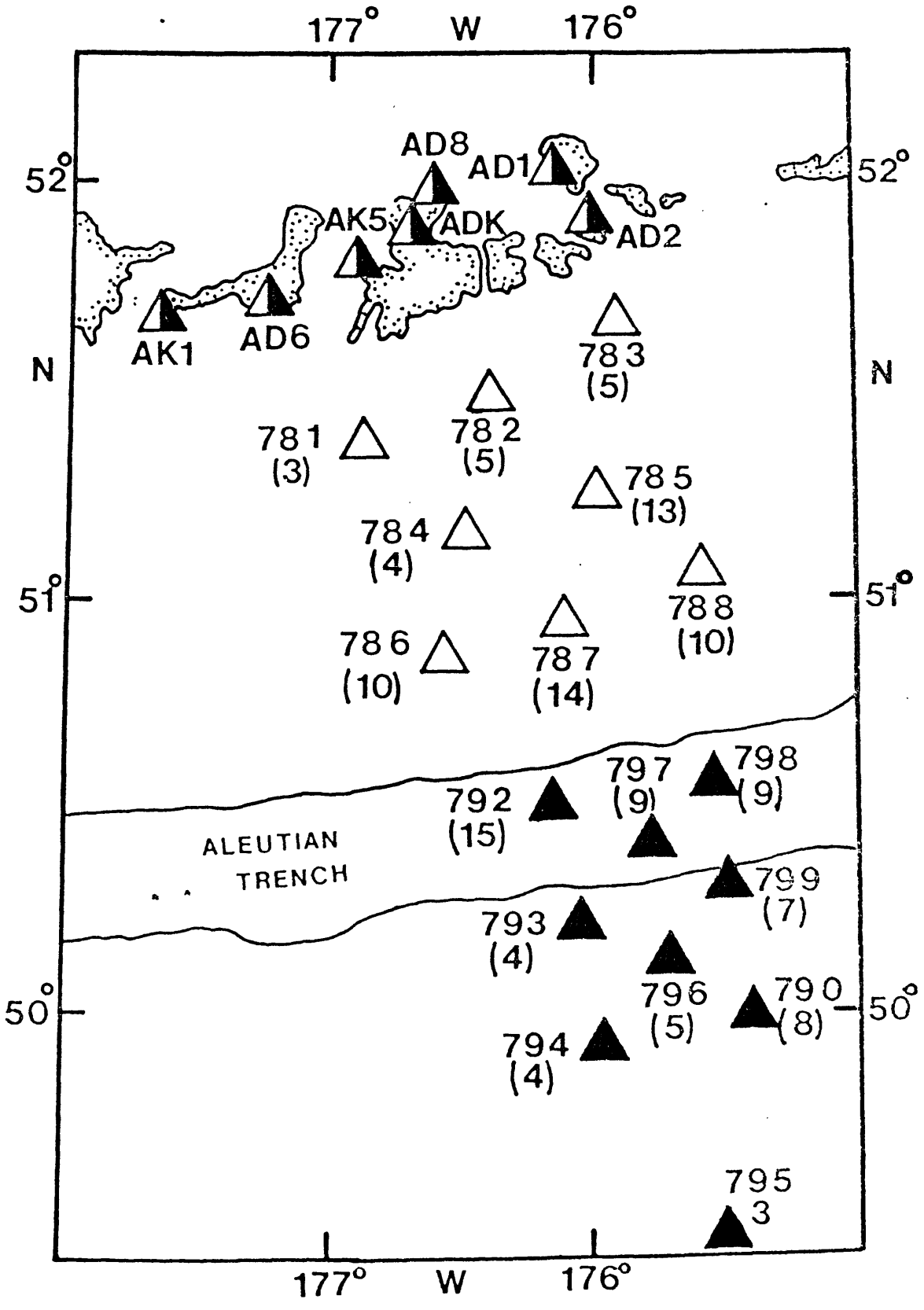

Figure 3-1: Locations of seismic stations providing data for the 1978 and 1979 experiments. Next to the station locations are the station name and (in parenthesis) the number of events per day recorded by the ocean-bottom stations. Filled triangles are the 1979 OBS stations, open triangles the 1978 OBS stations, and half-filled triangles are the Adak land stations.

landward of the trench. A second group lies between the volcanic islands and a line about 100 km landward of the trench axis. Events in this group are well recorded by the Adak land stations; the general pattern of the seismicity determined in the joint study using OBS stations as well as the land stations is the same as that already determined by the Adak network. Nearly all of the events located in the thrust zone by the OBS networks were also recorded by the more distant land network.

Location capability of the Adak land net. Several events which lay within the boundaries of the 1978 OBS network were well recorded by both island and OBS networks, and provide an excellent means of evaluating the location capabilities of the Adak land network. For 20 shallow events which were recorded by at least one station within 25 km of the epicenter, and which possessed RMS residuals smaller than 0.6 sec, the Adak network location averaged only 1.4 km south and 1.0 km west of the combined OBS/island location. The epicenters located by the Adak land network differed by as little as 0.6 km and as much as 11 km from the combined OBS/island locations, with a median difference of 3 km (Figure 3-2). The depths of these events as determined by the joint OBS/island network were considerably less clustered than the depths determined by the island network alone (Figure 3-3). In particular, note that while the island network determined 21 of 26 event depths between 18 km and 26 km, only five of the jointly determined depths were in this range.

The analysis of the joint OBS/island network locations strongly suggest that the land network has been systematically mislocating events with depths greater than about 70 km. In particular, for both the 1978 and 1979 experiments, the joint OBS/island locations seemed to be about 12 km northward of the island network locations for events with depths between 70 and 100 km.

Acceptability of standard Adak network velocity model. The flat-layer velo-

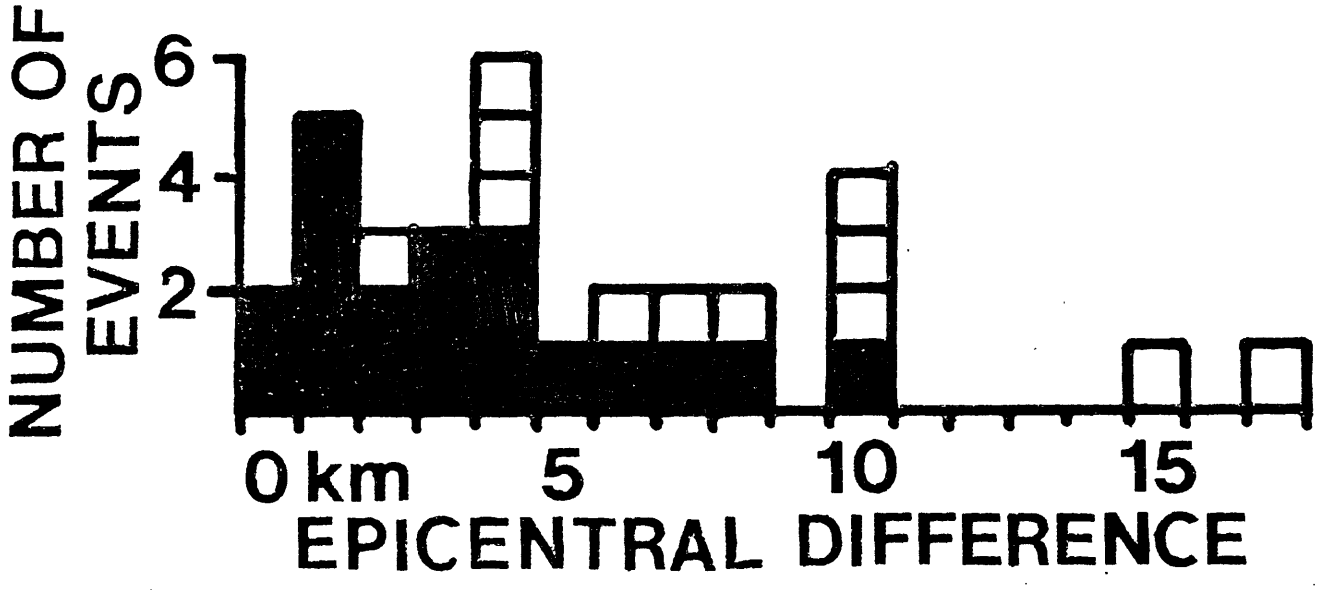

Figure 3-2: Distribution of distances between epicenters determined with arrivals from island station network and epicenters determined with arrivals from joint OBS/island network. Histogram includes only events with depths shallower than 50 km located between 21 June 1978 and 14 July 1978. Open squares are less well located events; i.e. their optimum location by the OBS/land station network has an RMS residual larger than 0.6 sec, or the epicenter lies 25 km or further from the nearest station in the OBS/island network.

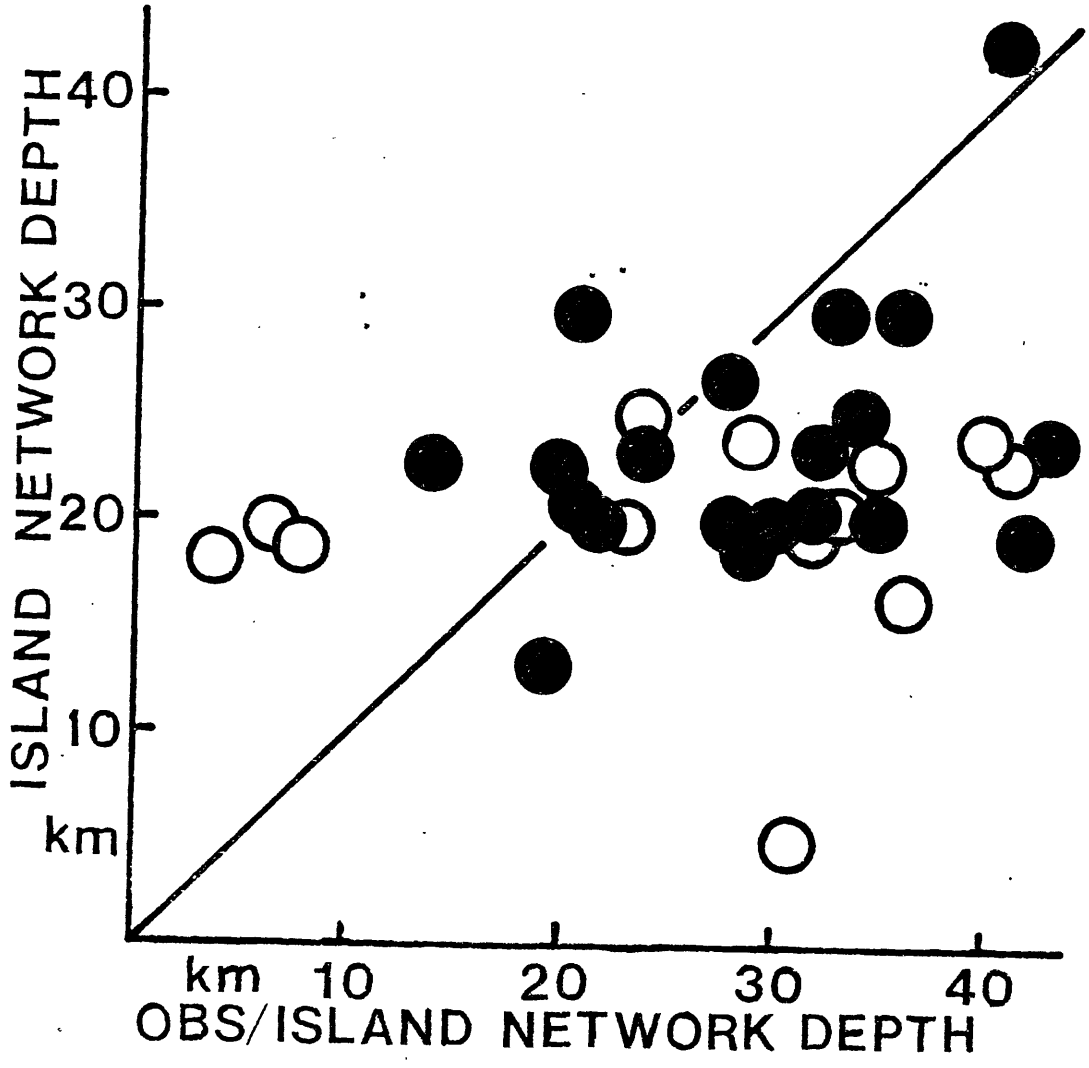

Figure 3-3: Focal depths of 1978 event as located by the island network and by the OBS/island network. These events are the same events that appear in Figure 3-2, with the open circles representing the less well located events.

city model used routinely for earthquake location using the Adak land station data is based on refraction study in the Bering Sea by Shor (1964). Experiments were made using the 1978 combined OBS/island data and several flat-layer velocity models, including the Adak standard one. No substantial improvement in the RMS residuals over those determined with the standard Adak velocity model was found with the other models used. The locations determined in the joint study were determined using two velocity models: one for the land and shallow OBS stations (the Adak standard model) and one for the OBS stations on the inner trench slope.

CHAPTER 4: PROCEDURES FOR COMPUTING FOCAL MECHANISMS FROM LOCAL $(SV/P)_z$ DATA

by Carl Kisslinger, Roger Bowman and Karl Koch[1)]

The principles underlying a method for determining the strike, dip and slip direction of an earthquake mechanism from the distribution of the ratio of the amplitudes of S and P waves at distances less than about 100 km were established in a recent paper, referred to in the following as Paper I (Kisslinger, 1980). The usefulness of the method was demonstrated by several examples, and some of the pitfalls likely to be encountered in applying it were explained. Computational procedures for routine analysis of typical local network data have now been developed. The availability of these computer programs has made it possible not only to process data rapidly and more thoroughly than was done previously, but also to carry out a variety of numerical experiments with real and synthetic data which serve to bring out further the subtleties and difficulties inherent in the technique.

The goal of the analysis is to find a focal mechanism which yields calculated ratios of the vertical component of SV to the vertical component of P in satisfactory agreement with the observed values of this quantity. The basis of the computations and the advantages in using this particular quantity, designated as $(SV/P)_z$, as the observed datum are explained in Paper I.

The dependence of $(SV/P)_z$, on the fault parameters is strongly non-linear and the "best-fitting" mechanism to a set of amplitude ratio data is not necessarily a well-constrained solution for the earthquake if all three parameters are free to vary arbitrarily. Some aspects of the inherent non-uniqueness have been discussed by Jones and Minster (1980). The analysis is, therefore, expedited by the imposition of some constraints on the starting solution on the basis of independent information. Some constraints are mandatory if a claim that the

1) Geophysical Institute, University of Karlsruhe, Federal Republic of Germany

solution of correct are for the event is to be made. In Paper I, the initial constraint was imposed by fixing the fault motion as either pure strike-slip or dip-slip. The decision was based on some combination of first-motion polarities and knowledge of the regional tectonics. This approach still appears to be a satisfactory way to get the best starting solution and choose among likely-looking alternatives that may come out of the processing.

Summary of the Theory.

The starting point for the calculations is the expression for the ratio of SV to P amplitudes generated by a point shear dislocation in an infinite, homogeneous medium. From Paper I, this is

$$(SV/P)_0 = \left[\frac{V_p}{V_s}\right]^2 \cot i_h \left[2 - \frac{(\cot\delta - \tan\delta)\sin\lambda \tan i_h \sin A + 2\sin\lambda + \csc\delta \cos\lambda \tan i_h \cos A}{D}\right] \quad (1)$$

where

$$D = \cos\lambda \cos A \sin i_h[-\sin i_h \sin A \sec\delta + \cos i_h \csc\delta] + \sin\lambda \sin i_h \cos i_h \sin A(\cot\delta - \tan\delta) + \sin\lambda(\cos^2 i_h - \sin^2 i_h \sin^2 A).$$

and

δ = dip of the fault

λ = direction of slip, measured in the fault plane from the strike

A = azimuth to the station, measured from the strike of the fault

i_h = take-off angle of the ray to the station at the source

V_p, V_s = P-wave and S-wave velocities

The effects of the various boundaries in the earth model on the ratio as observed at the surface must be considered. As explained in Paper I, one of several advantages of using the amplitude ratio rather than the absolute amplitudes is

that for a wide range of velocity contrasts and angles of incidence, the ratio of the SV to P transmission coefficients is close to 1, so that the effects of internal boundaries can be neglected. The validity of this assumption must be checked for each velocity model and range of distances used. Tables and figures such as those published by Costain, et al. (1963) and McCamy et al. (1962) are useful for this purpose.

The ratio of SV to P amplitudes in the interior must be converted to the ratio of the vertical amplitudes of these waves, as observed on the free surface. This is done by using equations derived by Gutenberg (1944). The factor by which $(SV/P)_0$ must be multiplied to obtain $(SV/P)_z$, for Poisson's ratio of 0.25, is shown in Figure 4-1. Three salient features are seen. For arrivals incident nearly vertically, at less than 30°, this correction is substantial and must be used. For angles of incidence in the range from about 30° to 37°, near the critical angle for SV-to-P conversion by reflection, the correction changes very rapidly with the angle of incidence. Data from stations within this range should be excluded from the analysis because the angle of incidence cannot be known with sufficient accuracy to make the required correction. Finally, for waves incident at between 37° and 80°, the factor is close to 1 and no great loss of accuracy results from neglecting the free surface effect.

The effects of inelastic attenuation on $(SV/P)_z$ are illustrated in Figure 4-2, for a vertical strike-slip fault at a depth of 6 km in a model consisting of a layer 2 km thick, in which the P-wave velocity is 4 km/sec, overlying a layer 13 km thick, with P-wave velocity 5.9 km/sec. These lie over a half-space, in which the velocity is 6.8 km/sec. If the dominant frequencies of the two body waves are the same, the effects are quite strong even at short distances, for frequencies typical of those seen with conventional microearthquake instrumentation. However, if the S-wave is characterized by a frequency somewhat lower than that of

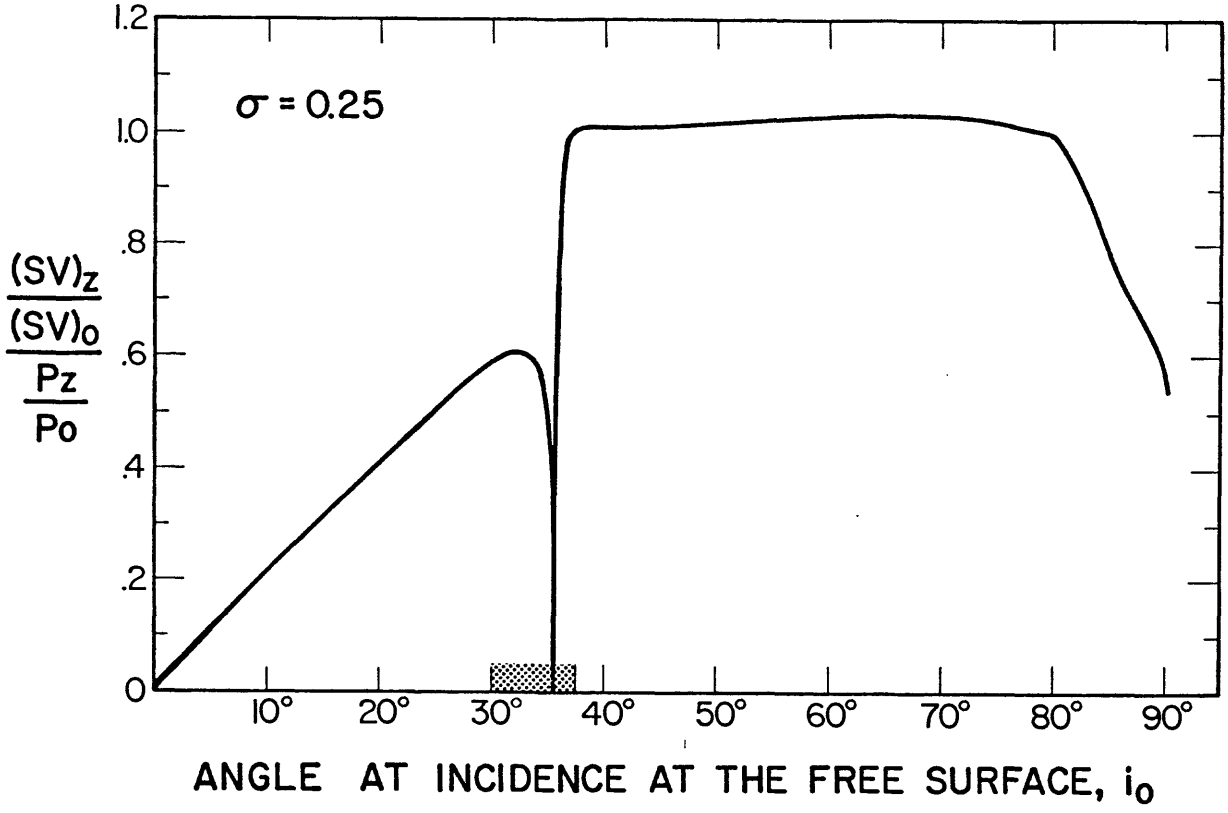

Figure 4-1: Factor to convert the ratio of the amplitudes of incident SV to incident P into the ratio of the amplitudes of the vertical components. The shaded section, 30° - 37°, is the range of angles near the critical angle for SV-to-P conversion by reflection in which data should be rejected. This is because of the the difficulty in determining the surface factor, which also involves a large phase shift, with sufficient accuracy.

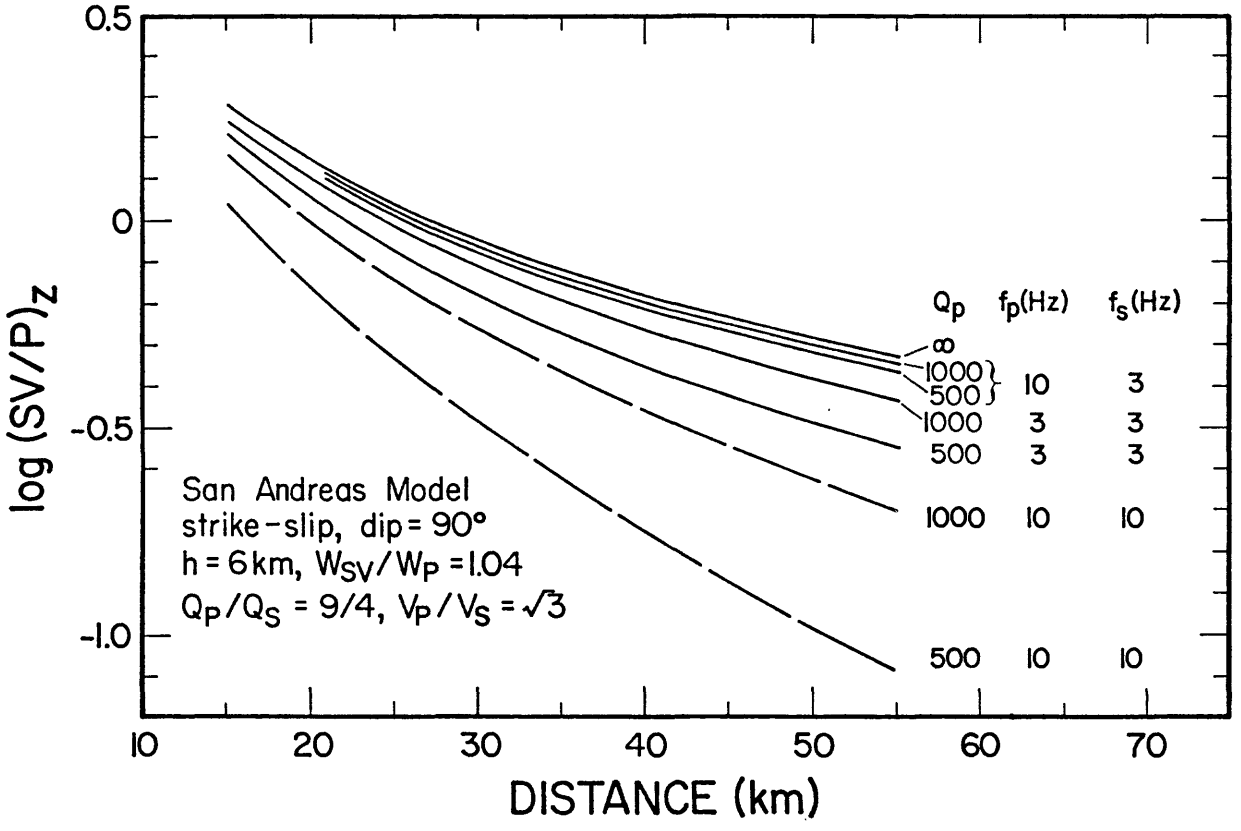

Figure 4-2: The effects of finite Q on $(SV/P)_z$ for a vertical strike-slip fault. Note the possibility of offsetting effects of frequency and Q for the second and third curves from the top.

P, the effects of the lower Q for S and the frequency offset in a way that makes the resulting change in $(SV/P)_z$ with distance hardly distinguishable from the case of perfect elasticity. As shown in Paper I, the central California data seemed to fit the theoretical values for infinite Q well enough, but the full investigation of the effects of Q on the focal mechanisms obtained by this method has not yet been done.

The Procedure.

The steps in the analysis are illustrated in block-diagram form in Figure 4-3. The required input is the best available hypocenter solution for the earthquake and a set of observations of $(SV/P)_z$ at the stations of the network. Errors in the position of the hypocenter, especially depth errors, cause errors in the focal mechanism, just as they do for more conventional methods. The method has so far been limited mostly to the use of upward traveling direct waves to the stations, but there is no reason in theory that downward traveling waves that reach the station after refraction or reflection cannot be used, as long as the P and S amplitudes that are compared have traveled the same path. The azimuth to each station and the take-off angle of the direct ray are read from the hypocenter solution. The corresponding angle of incidence at the free surface must be calculated and the free surface factor to give $(SV/P)_z$ taken from a curve, as in Figure 4-1, or a table.

The analyst must then decide if sufficient information is available to support a decision that the mode of slip is dominantly strike-slip or dip-slip, as discussed above. This decision will determine the outcome of the analysis. The problem is so strongly non-linear that the linear least-squares adjustment to be used subsequently cannot be relied on to compensate for a bad choice of the starting value of the slip direction. It is encouraging that in a number of cases where the evidence for a particular mode of faulting is very strong, the process

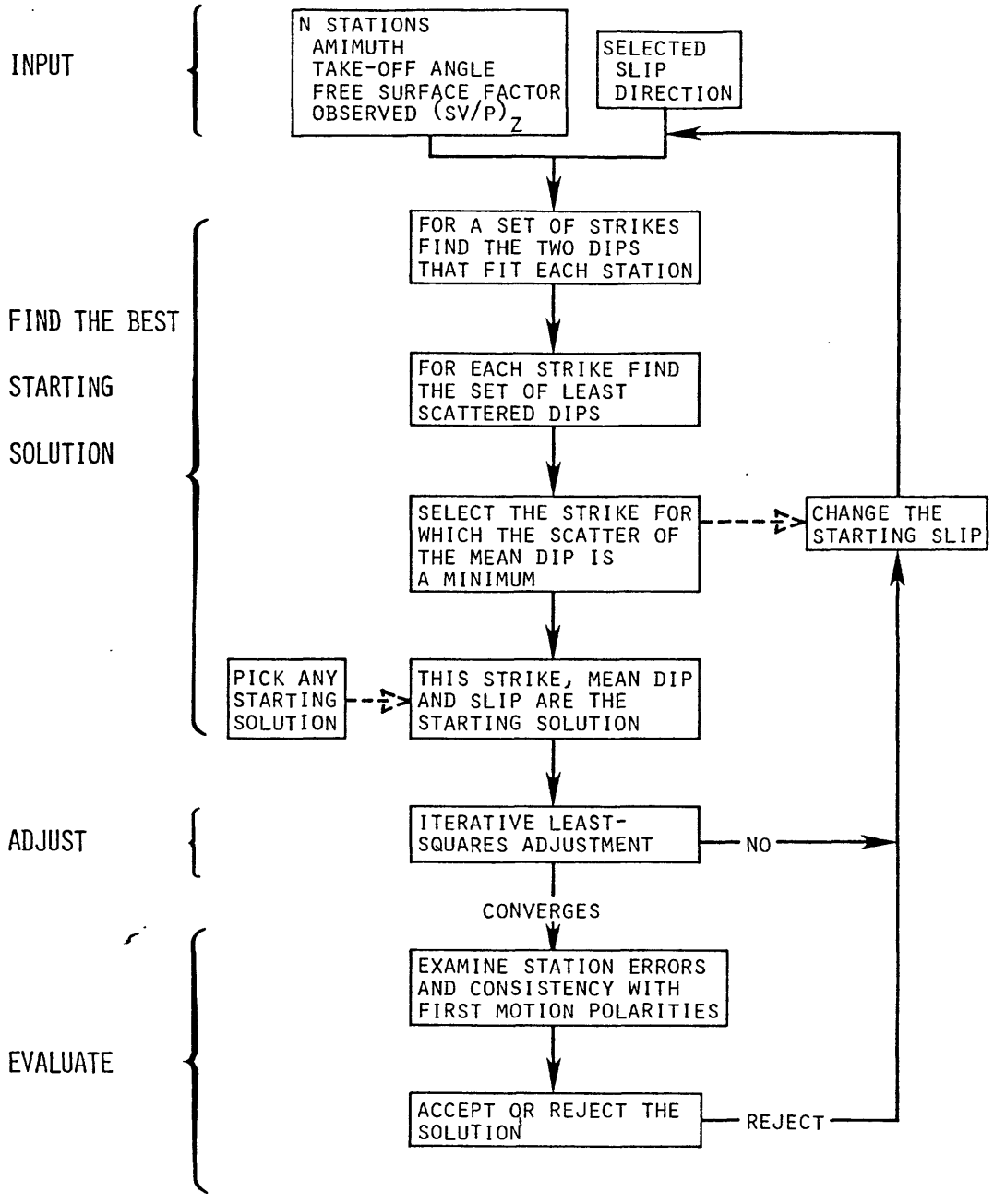

Figure 4-3: Flow diagram for the computational procedure.

would not converge when the wrong starting slip was intentionally used, so that no result, rather than a misleading one was obtained.

If there are no grounds for choosing either 0° or 90° as the most likely starting slip, the program can be used to try as starting values all slip angles, 0° through 180°, in selected small steps, in order to identify all plausible starting solutions. These solutions are those that have a fault dip with reasonably small scatter for some strike, for the given slip direction. This process consumes enough computer time that it is used only when there is no satisfactory alternative.

With the selected slip direction, the program then searches for the best-fitting solution, in the following sense. The basis theory, equation (1), shows that for a given slip direction and assumed fault strike, there are, generally, two values of the dip of the fault that will yield the observed value of $(SV/P)_z$, whatever it is. For an arbitrary fault strike, the pair of dips that correspond to the observed value of the amplitude ratio for one station will be totally different from the pair that satisfy some other station. However, if the data are good, there must be some value(s) of the strike for which one of the two dip values for each station is close to one of the two for all of the other stations.

The first step in the process is to find the two values of dip for each station for each strike, with the values of strike incremented in selected small steps (10° in the standard program). Because of numerical difficulties which may occur, stations are eliminated for the particular step in strike if the strike is the same as the station azimuth or, for the case of pure strike-slip, is 90° from the station azimuth.

In the search for the best starting solution, for pure strike-slip or pure dip-slip mechanisms only strikes from 0° to 180° need be tested, as the remaining value gives redundant information. However, if some other slip value is used as

the start, for example, the slip produced by the first computation, then all 360° must be searched.

The next step is to look through the array of strikes and 2n associated dip values for that strike for which one of the dips at each station is fairly close to one of the two values at all of the other stations. At this step it may be possible to identify and eliminate a station at which the amplitude data are bad, on the grounds that there is no strike value for which it yields a dip close to that of other stations. The n most clustered values of dip, one from each station, are selected, with the standard deviation of these values used as a measure of scatter. For some value of strike, the scatter of the best dips is the least. This strike and dip, with the selected slip direction, constitute the starting solution to which an iterative least-squares adjustment is applied. In many cases, a second strike-dip combination is present that is almost as good as the "best", i.e., the scatter of the dips is almost as small. This solution must also be examined.

The convergence criterion used is based on the sum squared errors of log $(SV/P)_z$ and this number is a measure of the goodness of fit of the final solution. However, it is also necessary to check the calculated values at the individual stations against the observations (i.e. the residuals). Otherwise good-looking solutions can be eliminated if they leave large residuals for reliable observations. The basic lack of uniqueness in the method can be at least partially overcome in this way. The obvious last step is to check the solution against the available first motion data in order to avoid inconsistencies and also to resolve the basic inability of this method to give the sense of slip.

This procedure has been programmed for the PDP 11/70 at CIRES. One run, including the search for the best starting solution and the least squares adjustment, takes about two minutes of CPU time for 6-10 stations.

Tests of the Procedure.

The procedure has been tested by more extensive processing of some of the earthquakes used in Paper I, application to some additional earthquakes and application to synthetic data. Because only the simplest computational and graphical techniques were used in Paper I, the slip directions were constrained to be either 0° or 90°. This severe restriction was removed and the effects of allowing arbitrary slip on the previous results examined.

Bear Valley Event. The first test was done on a set of data from an earthquake with magnitude 1.3 that occurred in Bear Valley California on April 9, 1971, at a depth of 6.8 km. This event was selected as typical of small Bear Valley events analyzed in Paper I and because it had produced $(SV/P)_z$ data at 14 stations, ranging in distance from 10 to 57 km. The station at 10 km (EKH) was eliminated because the angle of incidence at the free surface, 36.4°, was too near the critical value (Figure 4-1). The important result of this test was that the program, with no information other than the set of amplitude ratios and given a pure strike-slip start, found the San Andreas fault: fault strike = 130.°46 ± 1.°05; fault dip = 87.°37 ± 0.°71; slip direction = 0.°99 ± 1.°66. The strike of the surface trace of the fault at the epicenter is about 138° and in Paper I the mean dip determined for that strike and pure strike-slip was 89.°5 ± 3.°9.

Another significant finding for this earthquake was that a test of all slip directions showed that only a strike-slip solution was acceptable. A slip angle as small as 4° led to a non-convergent result, whereas 0°, and 2°, converged to the solution given above. Because we are quite confident that we know the focal mechanism for earthquakes on this fault, this result is especially comforting.

The solution for this earthquake comes closer to justifying a claim of uniqueness than any other event tested. This may be because it is also the event with the largest number of stations. Because the deployment of

instruments in the U.S.G.S. central California network places many stations close to the fault trace, a large number of the data points may come from places near the nodal line in the direction of the fault. To test whether this particular station distribution might be the reason for the apparently excellent result, another determination was made on the basis of a reduced data set from which all stations (4) with azimuths from the epicenter within 10° of the strike of the surface trace of the fault were deleted. The solution generated was: fault strike = 136.°82 ± 12.°08; dip = 88.°80 ± 0.°91; slip direction = 0.°40 ± 2.°18, still in good agreement with the known geology. Although the standard error of the strike is very large for this solution the quality of the result as measured by the summed squared errors of log $(SV/P)_z$ is better than for the solution with the full data set. This may be in part because the amplitudes at stations for which propagation is along the fault are distorted by either lateral velocity variations or fault-related differences in inelastic attenuation.

A less encouraging result is the discovery that if starting strikes and dips only slightly removed ($\approx$ 10°) from the best start found by the program are inserted arbitrarily, the process will converge to significantly different results. The existence of many local minima within the whole parameter space is confirmed by this, as is the dominant effect of the starting solution on the result obtained.

Darmstadt event. The magnitude 2.3 earthquake of June 7, 1979, near Darmstadt, Germany, also analyzed in Paper I, was subjected to a detailed examination using the computational procedure described here.

The systematic scan of all slip directions yielded seven acceptable solutions (sufficiently small scatter of the starting mean dip and the least squares adjustment converged). The search yields many more than seven slip directions with small scatter of the dip, but these converge by groups into one of the seven solu-

tions. Two of the seven were almost pure dip-slip, and five, primarily strike slip. The first-motion polarities were well-distributed in azimuth and ruled out all of the strike-slip solutions. The two dip-slip solutions were similar in strike, but differed in dip and slip direction: the conjugate pair for each solution are:

Solution 1: $strike_1 = 131.80$, $dip_1 = 45.29$, $slip_1 = 87.90$

$strike_2 = 308.81$, $dip_2 = 44.75$, $slip_2 = 92.13$

Solution 2: $strike_1 = 129.94$, $dip_1 = 36.99$, $slip_1 = 98.81$

$strike_2 = 320.91$, $dip_2 = 53.52$, $slip_2 = 83.42$

The subscripts '1' and '2' within each solution refer to the two conjugate fault planes. The method cannot distinguish between normal and reverse faulting, but the first motions show this fault to be normal. The solution for this earthquake published in Paper I, based on the assumption of pure dip slip, was 313°, 45.4°, or Solution 1 above. The two solutions found are almost indistinguishable in terms of strike and slip directions, but all of the measures of goodness of fit, mean error, summed squared errors, and standard errors of the three solution parameters all indicate that Solution 2 is slightly better.

Although the significance is not clear, it is worth noting that all seven of the solutions that emerged, strike- and dip-slip alike, each had one fault plane with a southeast-northwest dip, all but one dipping to the southwest. Whether a common feature of this kind is typical of the multiple solutions emerging from this procedure is not yet known, but the possibility of a trade-off between dip and slip direction for strikes within a fairly narrow band seems real.

Freiburg, Germany Sequence. On June 12, 1972, a sequence of six small earthquakes occurred between 00:30 and 06:22 UT, within 1-2 km of 48°01' N., 7°55'E, in a depth range from 15.8 - 17.6 km, as determined by the Geophysical Institute, University of Karlsruhe, under the direction of K.-P. Bonjer. The

duration magnitudes were 1.6-1.9. On June 14 one more very small event was located at almost the same place, just east of Freiburg, Baden-Wurttemberg, southwest Germany. A striking feature of the sequence is illustrated by the seismograms in Figure 4-4. A clear change in $(SV/P)_z$ for the sixth event compared to the first is seen at station FEL, with the change at SCH almost as certain. The amplitude ratio at BUH is not significantly different. These two earthquakes were located as being within one km of each other. A change in the orientation of the fault plane of event 6 compared to event 1 seems to be demanded by this observation.

Events number 1, 2, 3, and 6 were processed by the technique of this paper. Amplitude ratios at only 4 or 5 stations, but well distributed in azimuth, were available as input. Events 4 and 5 occurred only about 1 second apart, so their amplitudes could not be untangled. Event 7 was too small to use. All of the solutions are almost pure strike-slip on steeply dipping faults. It should be noted that the sparse first-motion polarities were added to the solution diagrams after the solutions were determined from amplitudes alone. In all cases, the first motions are consistent with the amplitude-ratio solutions. The slip angles given are consistent with the sense of motion required by the first motions. Events 1, 2 and 3 yielded almost identical solutions, with the mean values of the parameters approximately as follows:

$strike_1 = 38°$; $dip_1 = 81°$; $slip_1 = -1°$

$strike_2 = 308°$; $dip_2 = 809°$; $slip_2 = 171°$

This solution is illustrated for event 1 on Figure 4-4.

The solution for event 6, also shown on Figure 4-4, is (rounded off):

$strike_1 = 339°$; $dip_1 = 84°$; $slip_1 = -17°$

$strike_2 = 70°$; $dip_2 = 73°$; $slip_2 = 186°$

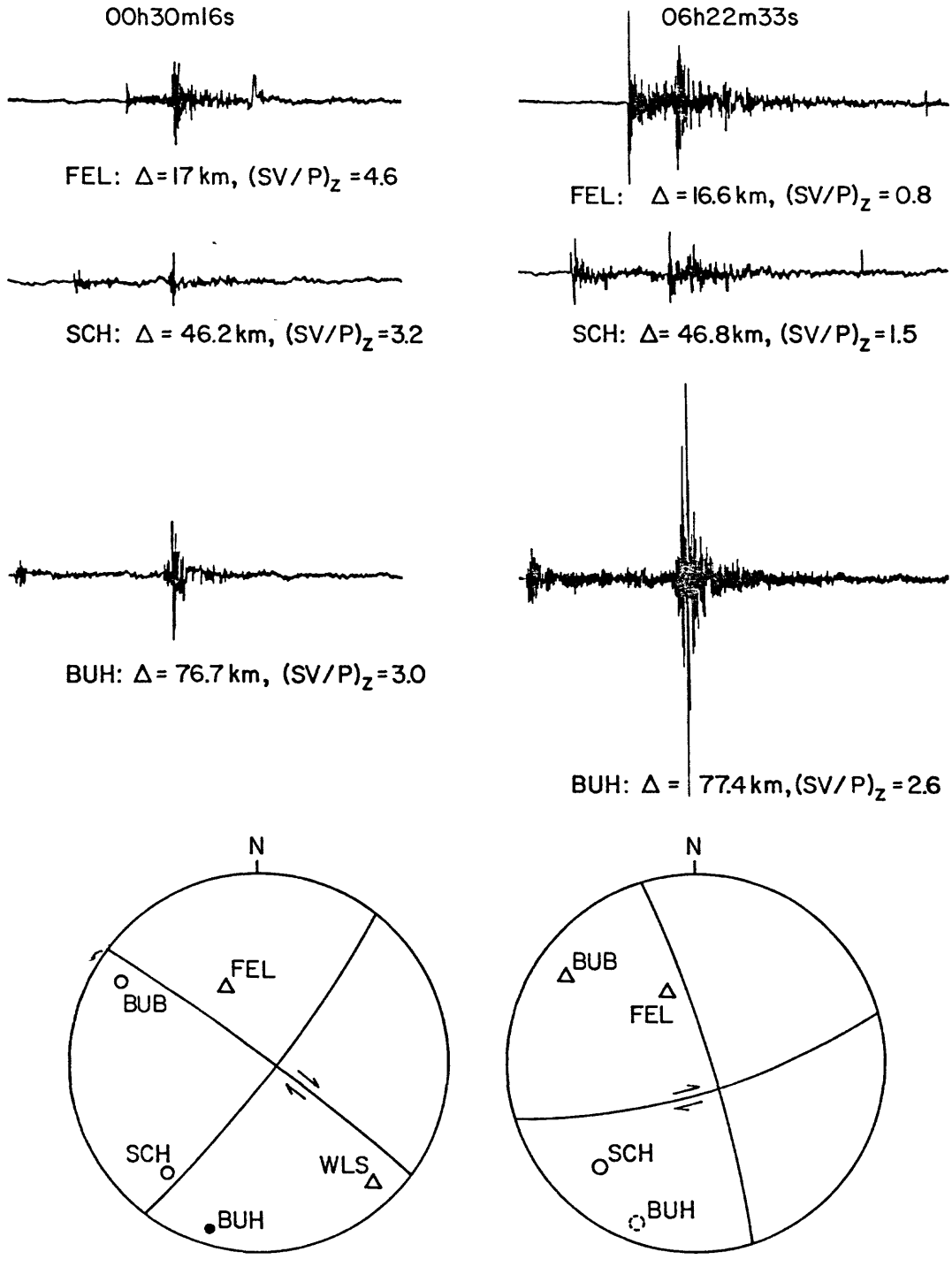

Figure 4-4: Vertical component seismograms and focal mechanisms for two events in the Freiburg sequence. The records at FEL show the remarkable change in $(SV/P)_z$ for two earthquakes six hours apart at almost the same place. The first motion polarities (circles for compression, triangles for dilatation, dot for uncertain) were added after the focal mechanisms had been calculated from the amplitude data.

The subscript '1' refers to the left-lateral fault, '2' to the right-lateral fault in each case, on the assumption that the sense of slip did not change as the fault plane rotated. The conclusion is that the fault plane rotated counterclockwise through about 58° between the first three and the sixth event in this little sequence. Although the seventh event, two days later, was too small to permit analysis, the seismogram at station FEL, with a large P-wave relative to S, indicates clearly that the focal mechanism is similar to that of event 6.

As a test, solutions for three of these earthquakes were sought starting from a pure dip-slip. The adjustment for event 1 diverged rapidly. For events 2 and 3 the process quickly moved to a strike-slip motion and slowly converged to solutions very similar to those found from a strike-slip start. This result was very encouraging.

This case shows, in addition to the geophysically interesting result that a pronounced change in fault plane strike can occur in a very limited volume within a short time, that even with few data, if these are of good quality and well-distributed in azimuth, this procedure will produce useful fault plane solutions for small earthquakes.

Synthetic Data. Values of $(SV/P)_z$ calculated from equation (1) have been used as input data to the program to test the internal consistency of the procedure. The fact that the procedure gives back the known input source, with zero error for the computed values of the three parameters, only proves that the program is doing what it is supposed to. Tests of this kind were useful, however, for not only debugging the program, but also for testing the algorithms used, especially the method of selecting one value of dip from the two found for each station for a given strike. Three methods were tried. The desired result is a selection of one dip for each station such that the standard deviation about the mean of the n values is a minimum. The method adopted starts with a cal-

culation of the mean of the 2n values and finds the single value at any station farthest from that mean. That extreme value is replaced by the other value for that station and the "better" value for that station is now fixed. The process is repeated until a value is chosen for each station. The mean and standard deviation are then calculated and filed. If the two values for a station are both very far from the final mean value, the method may pick the value farther from the final mean, so it has erred. However, in all such cases the "best-fitting" dip is so badly scattered that it and the strike that goes with it would not be considered as reasonable starting values, so the failure of the algorithm in these extreme cases does not lead to any error in the final result.

Tests on synthetic seismograms have yielded more ambiguous results. Synthetic seismograms for vertical strike-slip and 45° dip-slip faults, for distances typical of those used in the real earthquakes and for representative azimuths were calculated by M. Knecht of the Geophysical Institute, Karlsruhe using the program for the reflectivity method as developed by R. Kind (1978). Seismograms for some of the same cases were also calculated by D. Harvey of CIRES with his mode superposition program. The results of the two techniques were essentially indistinguishable.

The reflectivity calculations were carried out for $Q_\alpha = 1000$, $Q_\beta = 444$, dominant signal frequency of 3.2 Hz and a velocity model simulating the upper crust along the San Andreas fault in central California. The most thorough study was done for the case of the 45° dipping, dip-slip fault, at a depth of 6 km. The greatest difficulty was finding the S-wave on the synthetic seismograms. Beyond 15 or 20 km, the S amplitudes were much smaller relative to P than predicted by the dislocation theory. At some distances this was clearly due to interference of other arrivals, but the discrepancies are not yet understood. It was found that the agreement at all distances and azimuths was much better if the

"data", i.e., synthetic seismogram amplitudes, were corrected for Q_α, Q_β of 250, 111 instead of the values known to have gone into the calculations.

In spite of this disagreement of the synthesized $(SV/P)_z$, the fault mechanism obtained from the analysis was in satisfactory agreement with he the known input when the "data", corrected for Q, were used. The raw data, not Q-corrected, yielded a solution in poor agreement, strike = 308°, dip = 44.9°, slip = 110.8°, compared to the correct values of 360°, 45°, 90°. The data corrected for the known Q's gave a much better result: 177.9, 48.4, 88.7, with smaller standard errors on all three parameters (180° is, of course, the strike of the fault conjugate to 0° for dip-slip faulting). The fact that the synthetic amplitudes gave back the known input source mechanism when the correction for Q was made and not otherwise is taken as evidence that the overall procedure is basically correct.

The synthesized P arrivals agree with the radiation pattern predicted by the dislocation model, for both strike-slip and dip-slip faults. The relative amplitudes of the P arrivals as a function of distance and azimuth for the two modes of slip are as expected. The problem appears to be with the S waves. It is very likely that the smaller than expected S waves are the result of interference with multiply reflected waves in the low velocity surface layer. Further tests with different models are planned to try to resolve the apparent discrepancy.

The fact that a correction for finite Q was required to get a good result for the synthetics, while, for example, the data for Bear Valley, California are well-fit by the infinite Q theory, is probably because the frequency of both body waves is fixed at the same value in the synthetic seismograms, while a compensating lower frequency may dominate for the S waves in the real case (see Paper I and Figure 4-2).

Conclusions.

A convenient computational procedure has been developed for deriving the strikes, dip and slip direction of a fault from observations of $(SV/P)_z$ at short epicentral distances. A variety of tests demonstrated the validity of the approach and show that useful focal mechanism solutions can be obtained from sparse data, especially if the basic modes of slip is known independently. The inherent non-uniqueness of the technique is recognized, but this ambiguity can be overcome with added information that is often available.

This disagreement between values of $(SV/P)_z$ calculated by the method of this paper and those taken from synthetic seismograms is not resolved. Further tests, using a variety of velocity models will be done to try to find the source of the apparent conflict. It is encouraging that in spite of this disagreement, the focal mechanism obtained from the synthetic data is close to the known input.

CHAPTER 5: PRECURSORY CHANGES IN THE FOCAL MECHANISMS OF EARTHQUAKES PRECEDING A MAGNITUDE 4.6 EARTHQUAKE

by Roger Bowman

On July 15, 1980, an m_b=4.6 earthquake occurred at 37 km depth south of Adak Island (Figure 5-1). A search was made for seismicity precursors to this event. P wave first motions and $(SV/P)_z$ amplitude ratios of earthquakes which occurred within 20 km of the main event during the preceding 5 1/2 years were examined to detect any changes in focal mechanism preceding the July 15 earthquake.

Temporal changes in focal mechanism were not resolvable using P wave first motions. However, several important observations could be made from the first motion data. A plausible fault plane solution for an m_d=3.5 earthquake which occurred on May 8, 1980 at virtually the same hypocenter as the July 15 earthquake is shown in Figure 5-2. The fault plane solution is not well constrained; a pure thrust mechanism has been assumed, consistent with teleseismically determined mechanisms and available first motions. Throughout the period studied, stations AD1 and AD2 showed the greatest variation of first motion polarity. AD3 was in the compressional quadrant for 90% of the events studied, while all the stations shown in the dilatational quadrant in this figure were in that quadrant for 90% of the events studied. Clearly, a nodal plane passes through the eastern half of the network.

Dislocation theory predicts that a small change in orientation of the nodal plane should produce a large change in $(SV/P)_z$ amplitude ratio at station AD1 because of its position near a nodal plane (Kisslinger, 1980). Conversely, AD6 is not near a nodal plane, and should be relatively insensitive to small changes in the orientation of the focal mechanism. P and SV amplitude ratios were measured from seismograms of more than 100 small earthquakes (m_d < 2.1) which occurred between August 1974 and October 1980. During a seven month period

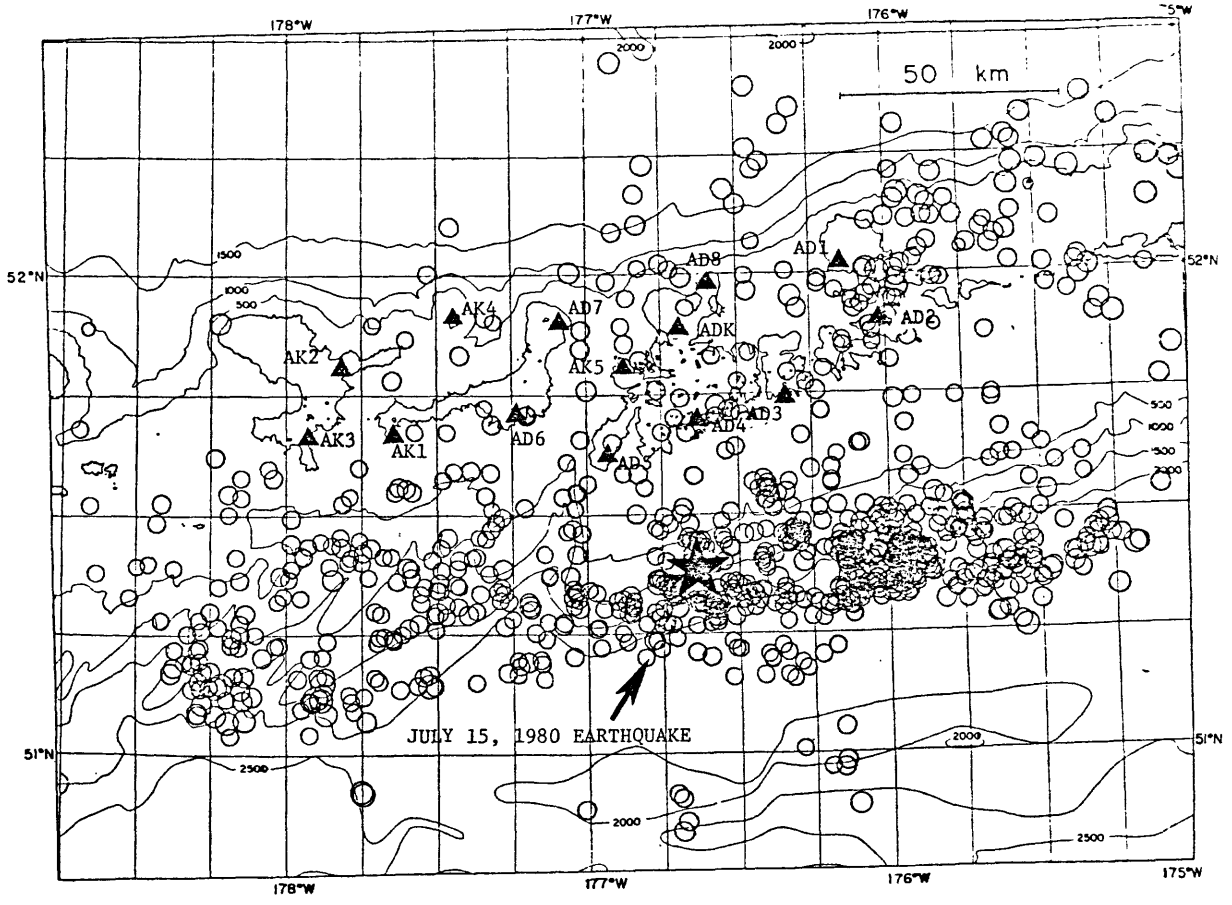

Figure 5-1: Map view of seismicity from August 1974 through December 1978 in which only free-depth-solutions for events with duration magnitude greater than or equal to 2.2 (m_b about 2.7) are plotted. Bathymetric contours are at 500 fathom intervals. Seismograph stations of the Adak local network are indicated by filled triangles. The location of the July 15, 1980, m_b 4.6 earthquake is indicated by the solid star.

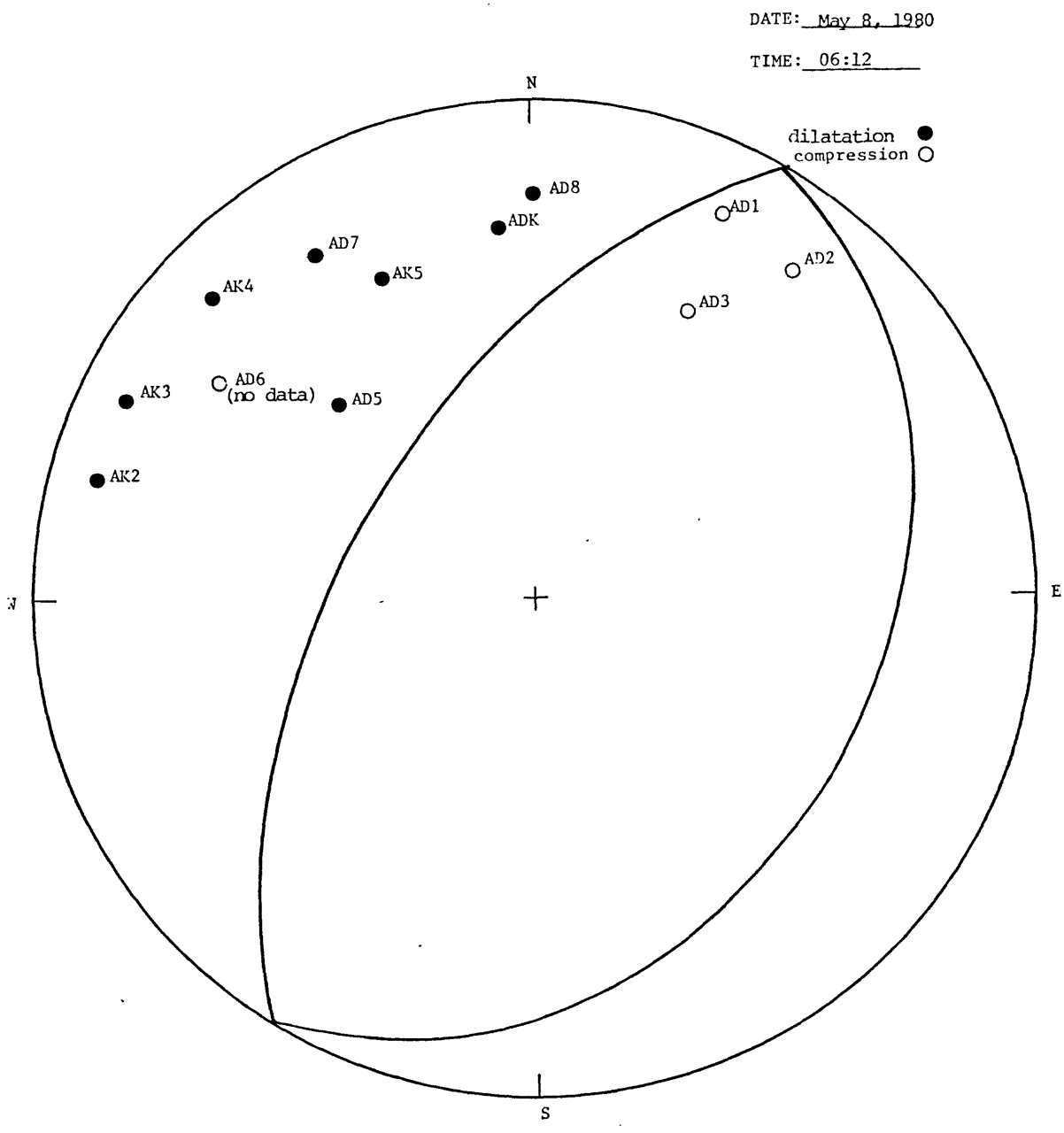

Figure 5-2. Upper hemisphere projection fault plane solution for the May 8, 1980, m_d 3.5 earthquake. Dilatations are shown as filled circles and compressions as open circles.

preceding the July 15 earthquake, the log $(SV/P)_z$ amplitude ratio at station AD1 changed from 0.3 to 0.6. During the same period, the log amplitude ratio at AD6 remained constant at 0.2.

A plot of log $(SV/P)_z$ amplitude ratio at stations AD1 and AD6 with respect to time is shown in Figure 5-3. The increase in data points in 1979 and 1980 is the result of concentration on this time period for this study and the quiet periods in 1975-76 and 1977-78 are a product of instrumentation failure. There was a dramatic shift in amplitude ratio at AD1 in December 1979. In contrast, the amplitude ratio observed at AD6 was constant throughout the six year period. The scatter of the depth of the events studied increased in 1979 and 1980. This is an artifact of sampling, not of a change in seismicity rate. In order to delineate the anomaly, more events were examined during this period. However, a possible relationship between depth and amplitude ratio should be considered.

Amplitude ratio as a function of depth at stations AD1 and AD6 is shown in Figures 5-4 and 5-5. The log $(SV/P)_z$ value observed at station AD1 is clustered by time period and depth in Figure 5-6. For example, in the depth slice from 30 to 50 km, close to the 37 km depth of the July 15 earthquake, background events and aftershocks are clustered between 0.1 and 0.5 log amplitude ratio while the pre-shocks are between 0.5 and 1.1. Thus, it appears that the temporal change of amplitude ratio at AD1 is not an artifact of depth. AD6 does not show a systematic differentiation of pre-shocks from the background period or a systematic relationship of depth and amplitude ratio (Figure 5-6).

A plot of log amplitude ratio with respect to time for depth intervals of 0-30 km and 30-50 km (Figures 5-6 and 5-7) show that the amplitude ratio change occurred in both depth intervals. In Figure 5-7, it appears that the anomalous amplitude ratio period ended considerably before the July 15 earthquake. This

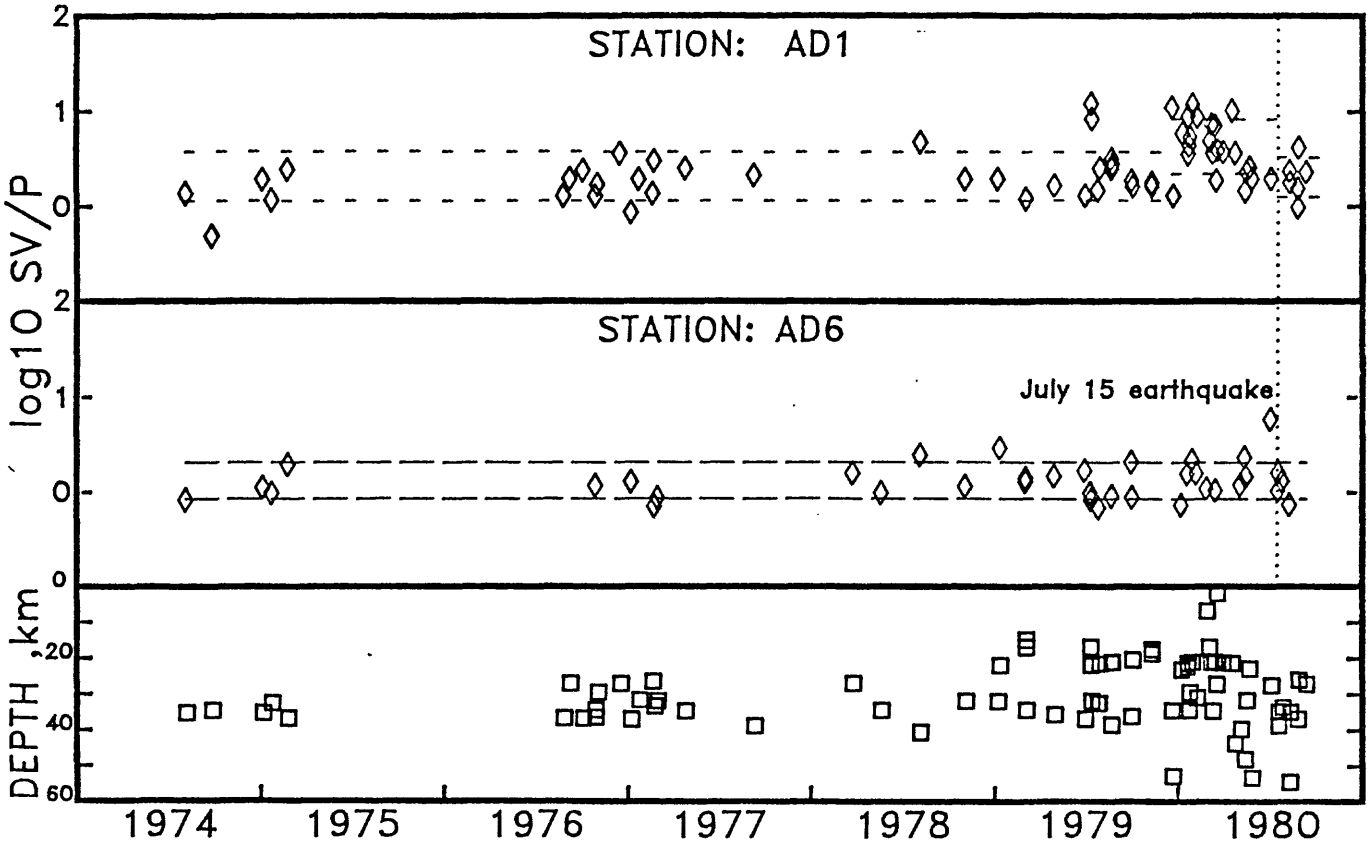

Figure 5-3: Graph of log $(SV/P)_z$ amplitude ratio as a function of time at stations AD1 and AD6. Depths of events with amplitude ratio measurements are shown in the lower frame. Dashed lines through the amplitude data are one standard deviation from the mean. The time of occurrence of the July 15 earthquake is indicated by a vertical dotted line.

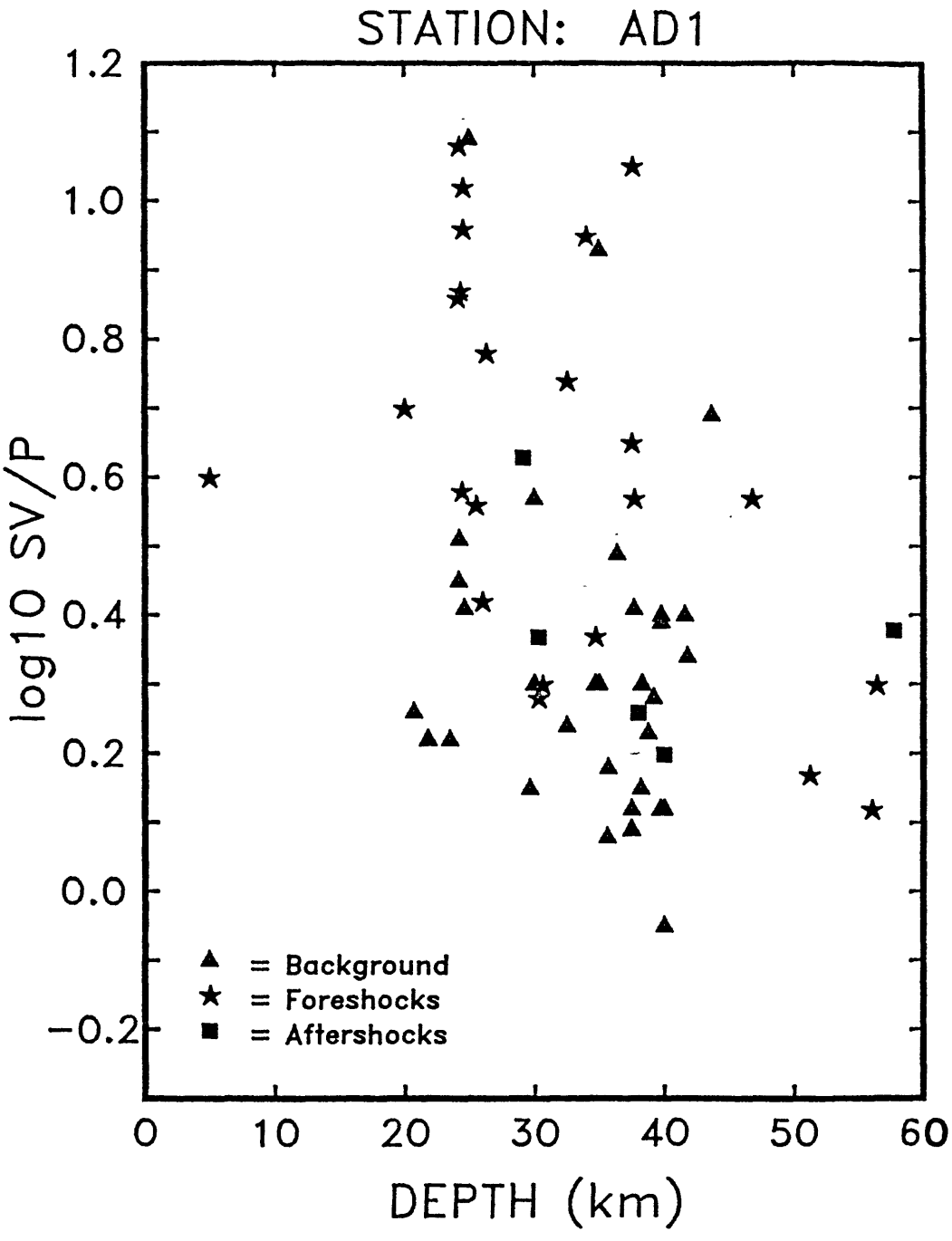

Figure 5-4: Graph of log $(SV/P)_z$ amplitude ratio at station AD1 as a function of depth. Earthquakes which occurred between August 1974 and December 17, 1979 are shown as triangles, between December 17, 1979 and July 15, 1980, as stars, and between July 15 and October 1980, as squares.

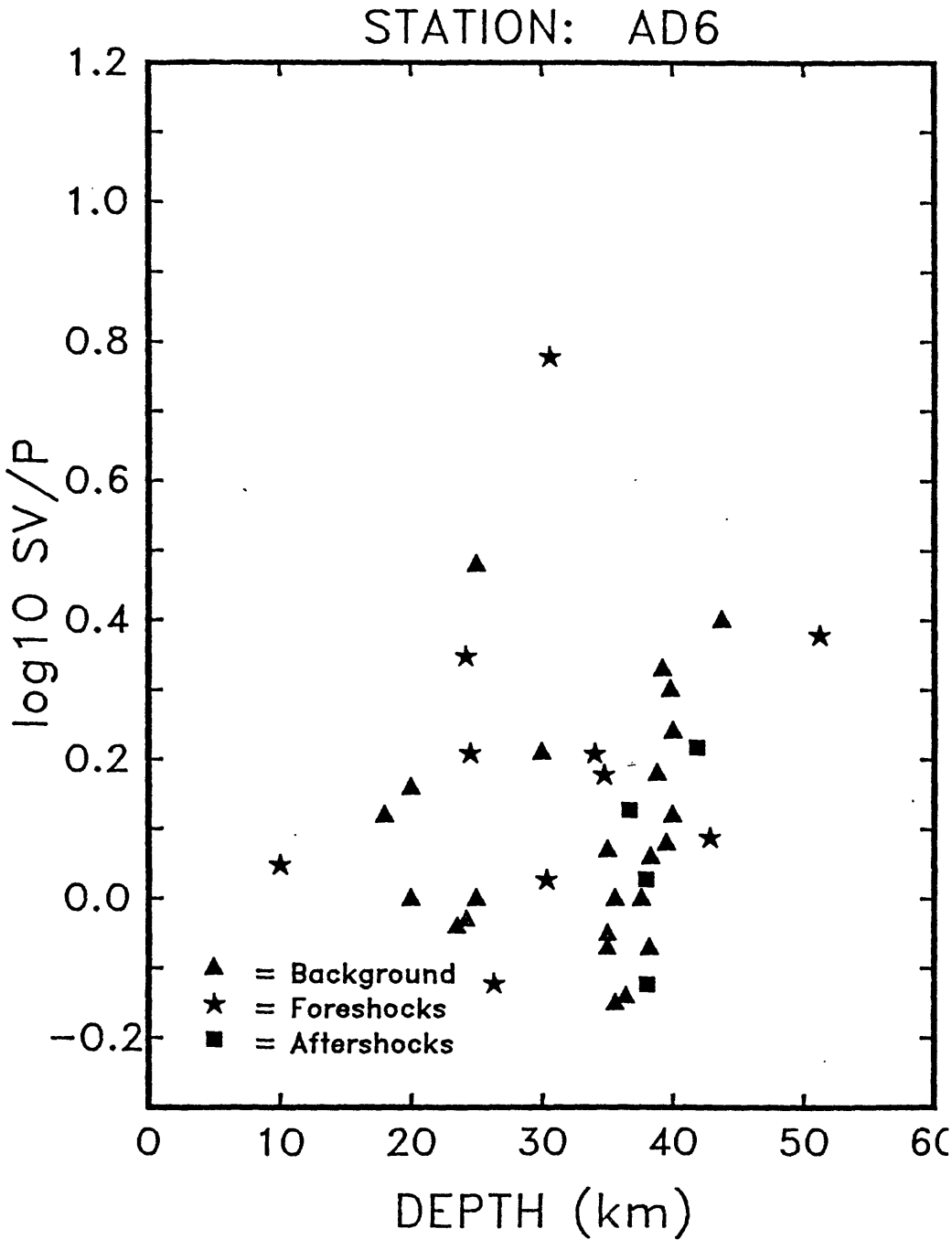

Figure 5-5: Graph of log $(SV/P)_z$ amplitude ratio at station AD6 as a function of depth. Symbols are as in Figure 5-4.

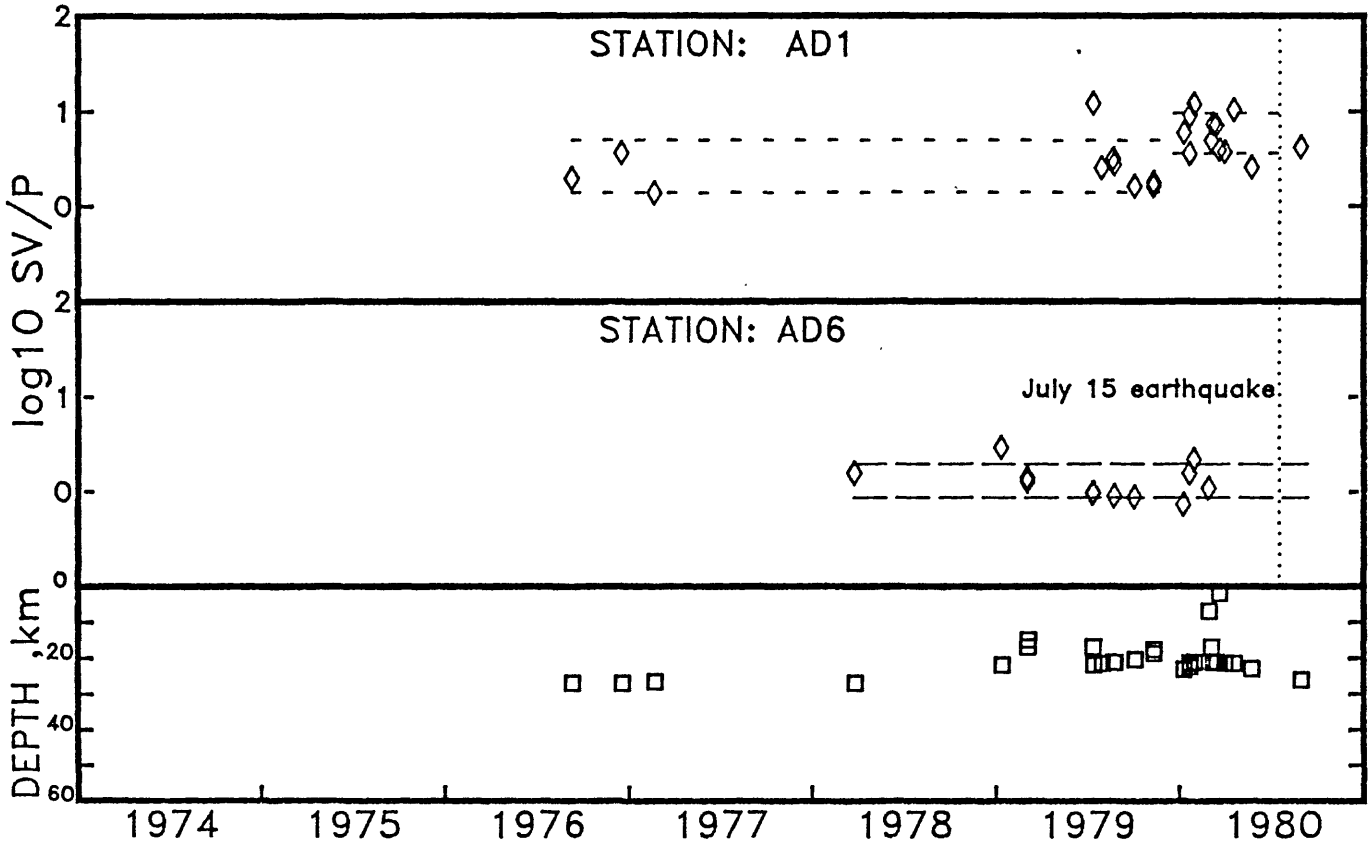

Figure 5-6: Graph of log $(SV/P)_z$ amplitude ratio as a function of time for earthquakes of depth 0 - 30 km.

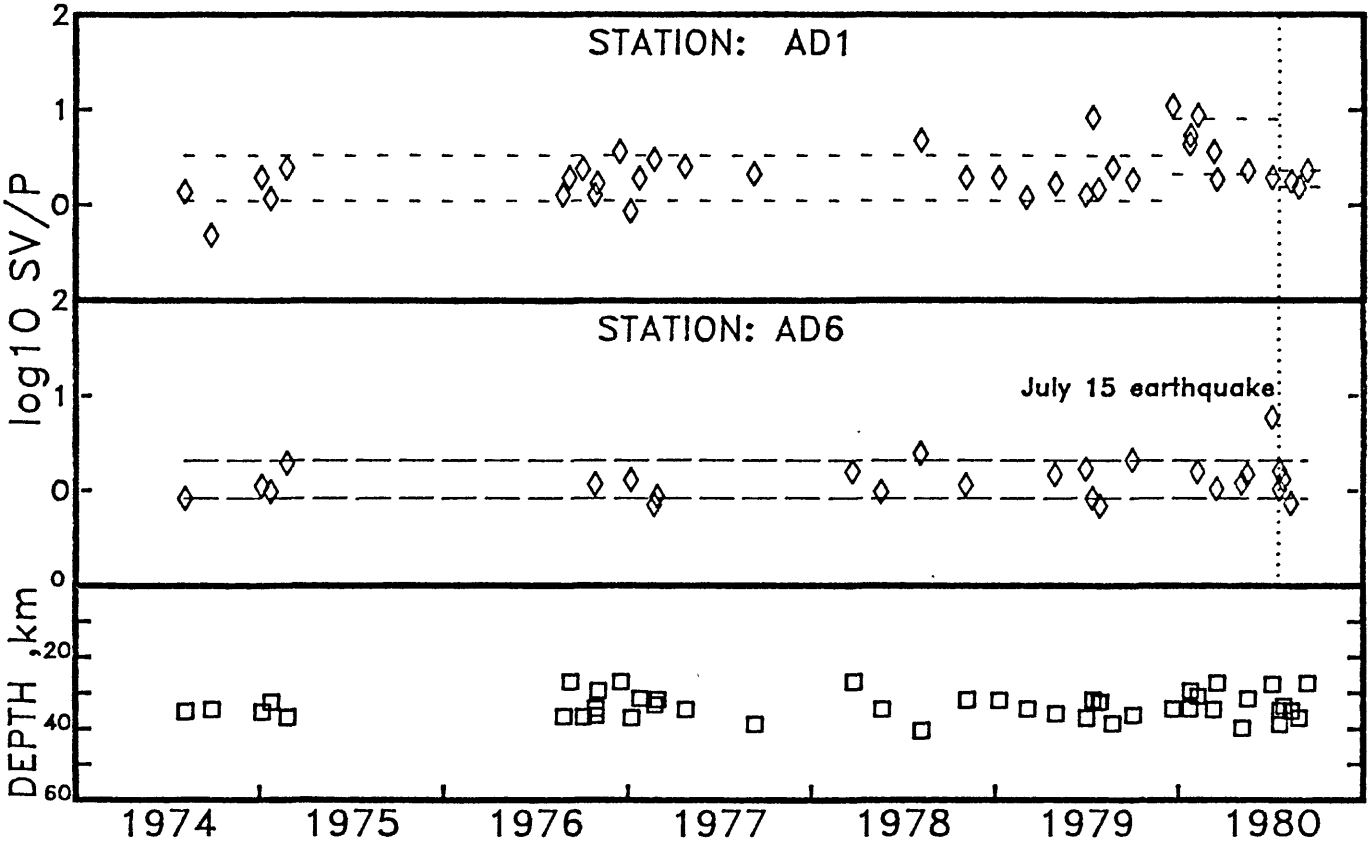

Figure 5-7: Graph of log $(SV/P)_z$ amplitude ratio as a function of time for earthquakes of depth 30 - 50 km.

figure suggests that the anomalous behavior may have culminated with the m_d=3.5 May 8 earthquake. The aftershocks have clearly returned to the background level of amplitude ratio.

A clockwise rotation of 15°-20° of the thrust mechanism shown in Figure 5-2 could account for the change in observed amplitude ratio at AD1 and the stability of the ratio at AD6. The inferred rotation of focal mechanism prior to the July 1980, February 1976 (Engdahl and Kisslinger, 1977) and November 1977 (Billington et al, 1980) earthquakes are shown in Figure 5-8. These three cases together suggest that a reorientation of focal mechanism of small earthquakes occurs as part of the preparation process for larger earthquakes in the Adak thrust zone.

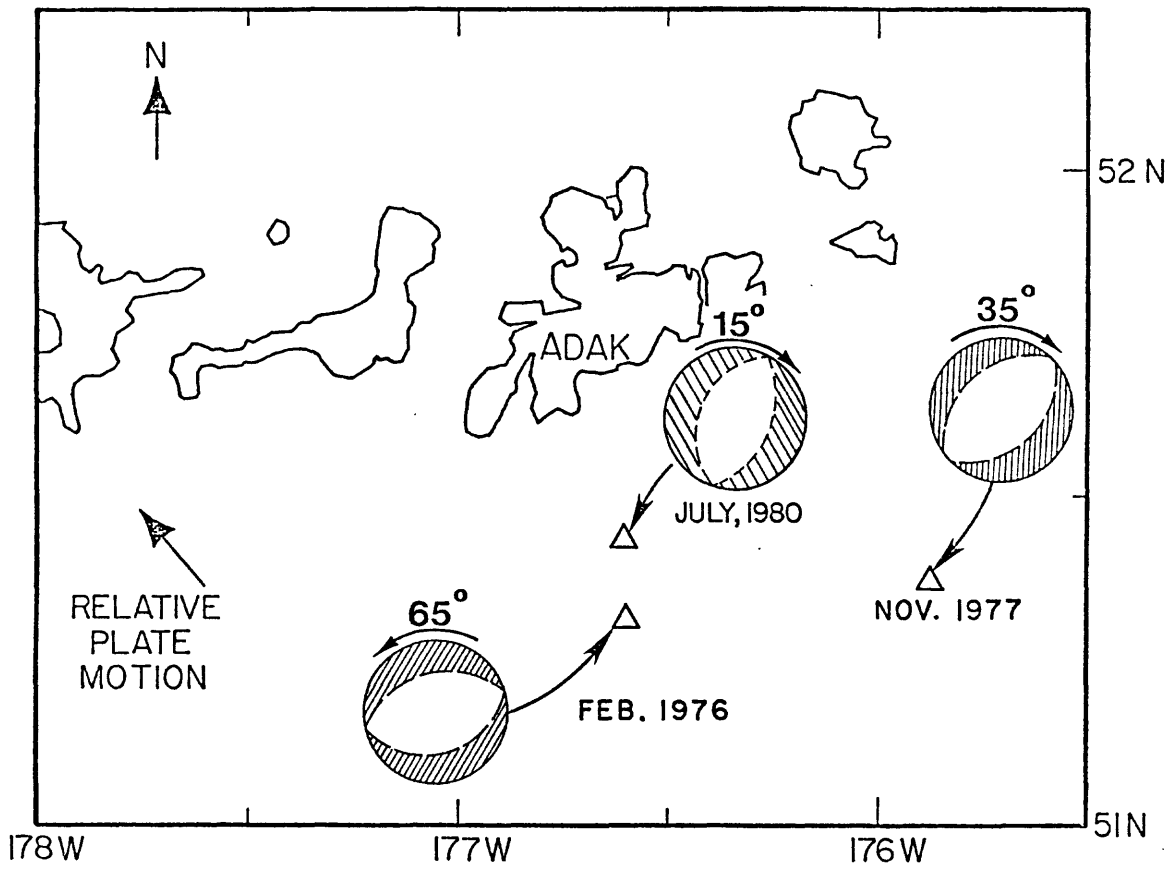

Figure 5-8: Inferred rotation of focal mechanisms before three earthquakes in the Adak seismic zone. The February 1976 interpretation is from Engdahl and Kisslinger (1977), the November 1977 one from Billington et al., (1981) and the July 1980 one from Bowman and Kisslinger (1981).

REFERENCES

Billington, S., E.R. Engdahl, and S. Price (1981). Changes in the seismicity and focal mechanism of small earthquakes prior to an M_S 6.7 earthquake in the central Aleutian island arc, in press, Ewing Series Vol. 4: **Earthquake Prediction.**

Bowman, R., and C. Kisslinger (1981). Changes in focal mechanism of small earthquakes before an m_b 4.6 earthquake in the central Aleutian seismic zone (abstract), **Earthquake Notes, 52**, 69.

Costain, J.K., K.L. Cook and S.T. Algermissen (1963). Amplitude, energy, and phase angles of plane SV waves at this application to earth crustal studies, **Bull. Seism. Soc. Amer, 53**, 1039-1074.

Engdahl, E.R., and C. Kisslinger (1977). Seismological precursors to a magnitude 5 earthquake in the central Aleutian islands, **J. Phys. Earth, 25**, 6243-S250.

Frohlich, C., J.G. Caldwell, A. Malahoff, G.V. Latham, and J. Lawton (1980). Ocean bottom seismograph measurements in the central Aleutians, **Nature, 286**, 144-145.

Gutenberg, B. (1944). Energy ratio of reflected and refracted seismic waves, **Bull. Seism. Soc. Amer., 34**, 85-101.

Jones, C. and B. Minster (1980). Local earthquake focal solutions using P-SV amplitude information, (abstract), **EOS, 61**, 1028.

Kind, R. (1978). The reflectivity method for a buried source, **Journal of Geophysics, 44**, 603-612.

Kisslinger, C. (1980). Evaluation of S to P amplitude ratios for determining focal mechanisms from regional network observations, **Bull. Seism. Soc. Amer., 70**, 999-1014.

McCamy, K. R. Meyer and T.J. Smith (1962). Generally application solutions of

Zoeppertz's amplitude equations, **Bull. Seism. Soc. Amer., 52**, 923-955.

Shor, G.C. (1964). Structure of the Bering Sea and the Aleutian Ridge, **Marine Geol., 1**, 213-216.